RESEARCH ARTICLE SUMMARY

NATURAL PRODUCTS

Structure elucidation of colibactin and its DNA cross-links

Mengzhao Xue*, Chung Sub Kim*, Alan R. Healy, Kevin M. Wernke, Zhixun Wang, Madeline C. Frischling, Emilee E. Shine, Weiwei Wang, Seth B. Herzon†, Jason M. Crawford†

INTRODUCTION: Research on the human microbiome has revealed extensive correlations between bacterial populations and host physiology and disease states. However, moving past correlations to understanding causal relationships between the bacteria in our bodies and our health remains a challenge. A well-studied human-bacteria relationship is that of certain gut *Escherichia coli* strains whose presence correlates with colorectal cancer in humans. These *E. coli* damage host DNA and cause tumor formation in animal models, and this genotoxic phenotype is thought to derive from a secondary metabolite—known as colibactin—that is synthesized by the bacteria. Because colibactin's biosynthetic pathway is only partially resolved, the complete structure of colibactin has remained unknown for more than a decade. Similarly, because colibactin is unstable and is produced in vanishingly small quantities, it has yet to be isolated and characterized by means of standard spectroscopic methods.

RATIONALE: Determining colibactin's chemical structure and related biological activity will allow researchers to determine whether the metabolite is the causal agent underlying many colorectal cancers. To that end, we used an interdisciplinary approach to overcome the challenges that have impeded determination of colibactin's structure. Inspired by an earlier study that showed that colibactin-producing bacteria cross-link DNA, we used DNA as a probe to isolate colibactin from bacterial cultures. Using a combination of isotope labeling and tandem mass spectrometry analysis, we deduced the structure of the colibactin residue when bound to two nucleobases. This information allowed us to then identify and characterize colibactin in bacterial extracts and to identify plausible biosynthetic precolibactin precursors. Last, we developed a method to recreate colibactin in the laboratory and thereby confirm these structure-function relationships.

RESULTS: Colibactin is formed through the union of two complex biosynthetic intermediates. This coupling generates a nearly symmetrical structure that contains two electrophilic cyclopropane warheads. We found that each of these residues undergoes ring-opening through nucleotide addition, a determination that is consistent with earlier studies of truncated colibactin derivatives and the observation that colibactin-producing bacteria cross-link DNA. Using genome editing techniques, we were able to show that the production of colibactin's precursor, precolibactin 1489, requires every biosynthetic gene in the colibactin gene cluster, implicating it as being derived from the long-elusive and now completed biosynthetic pathway. Because natural colibactin remains non-isolable, the chemical synthetic route to colibactin we developed will allow researchers to probe for causal relationships between the metabolite and inflammation-associated colorectal cancer.

ON OUR WEBSITE

Read the full article at http://dx.doi.org/10.1126/science.aax2685

CONCLUSION: These studies reveal the structure of colibactin, which accounts for the entire gene cluster encoding its biosynthesis, a goal that has remained beyond reach for more than a decade. The complete identity of colibactin has been a missing link in determining whether and how often colibactin is the causal agent underlying colorectal cancers. The interdisciplinary approach we used—marrying chemical synthesis, metabolomics, and probe-mediated natural product capture—may be applicable toward other spectroscopically intractable metabolites that are implicated in disease phenotypes but are currently undetected in the enormous chemical space encoded by the microbiome. Our studies represent a substantial advance toward our understanding of causative rather than correlative relationships between the gut microbiome and human health. ■

The list of author affiliations is available in the full article online.
*These authors contributed equally to this work.
†Corresponding author. Email: jason.crawford@yale.edu (J.M.C.); seth.herzon@yale.edu (S.B.H.)
Cite this article as M. Xue *et al.*, *Science* **365**, eaax2685 (2019). DOI: 10.1126/science.aax2685

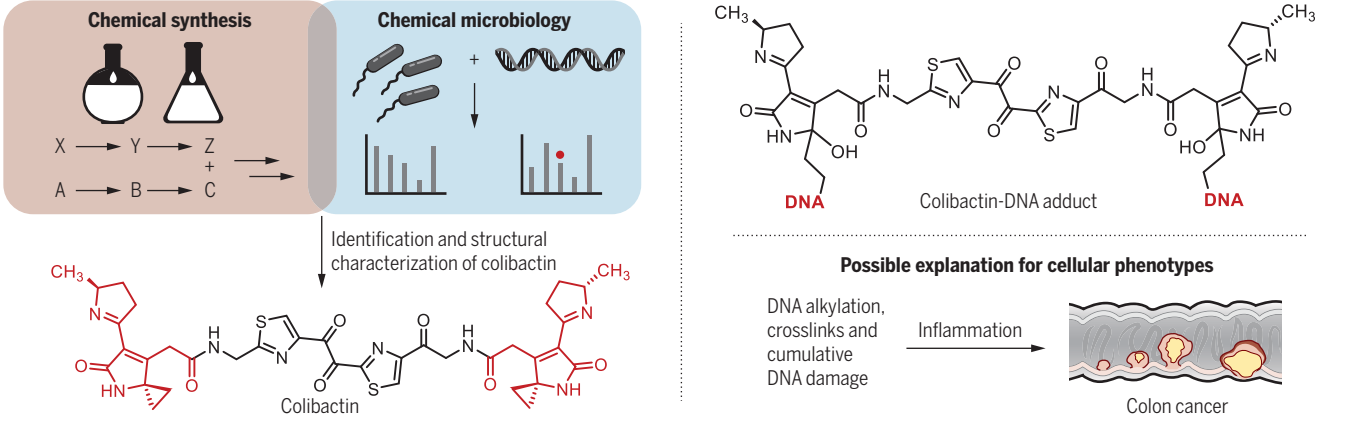

Molecular basis for colibactin-associated colorectal cancers. (Left) Parallel, complementary approaches of total synthesis and tandem mass spectrometry–guided labeled DNA analysis identified the colibactin metabolite responsible for DNA cross-links. Elements highlighted in red are the two electrophilic cyclopropane motifs that are the site of DNA adduction. (Right) With structural information in hand, we can now assess the molecular pharmacophores responsible for colibactin-associated inflammation and carcinogenesis.

RESEARCH ARTICLE

NATURAL PRODUCTS

Structure elucidation of colibactin and its DNA cross-links

Mengzhao Xue[1]*, Chung Sub Kim[1,2]*, Alan R. Healy[1,2]†, Kevin M. Wernke[1], Zhixun Wang[1]‡, Madeline C. Frischling[1], Emilee E. Shine[2,3], Weiwei Wang[4,5], Seth B. Herzon[1,6]§, Jason M. Crawford[1,2,3]§

Colibactin is a complex secondary metabolite produced by some genotoxic gut *Escherichia coli* strains. The presence of colibactin-producing bacteria correlates with the frequency and severity of colorectal cancer in humans. However, because colibactin has not been isolated or structurally characterized, studying the physiological effects of colibactin-producing bacteria in the human gut has been difficult. We used a combination of genetics, isotope labeling, tandem mass spectrometry, and chemical synthesis to deduce the structure of colibactin. Our structural assignment accounts for all known biosynthetic and cell biology data and suggests roles for the final unaccounted enzymes in the colibactin gene cluster.

Research on the human microbiota has now established a large number of correlative relationships between bacterial species and host physiology or disease. However, deriving causal relationships from correlations or associations remains challenging (*1*). Evidence suggests that molecular-level approaches may ultimately be required to unveil many causal relationships in the microbiome; success here will illuminate therapeutic strategies to treat disease and improve human health (*2*). Toward this end, a large amount of research has been devoted to studying certain strains of Enterobacteriaceae that contain a 54-kb biosynthetic gene cluster (BGC) termed *clb* (also referred to as *pks*). The *clb* gene cluster encodes the biosynthesis of a nonproteogenic metabolite known as colibactin. *Clb*$^+$ *Escherichia coli* are commonly found in the human colon (*3*, *4*), induce DNA damage in eukaryotic cells (*5*, *6*), promote tumor formation in mouse models of colorectal cancer (CRC) (*7*–*9*), and are more prevalent in CRC patients than healthy subjects (*7*, *10*). These findings have been attributed to colibactin, but experiments designed to test this hypothesis have been impossible to conduct because colibactin does not appear to be isolable, and its structure has remained incompletely defined (*11*–*15*). Understanding the full structure of colibactin will lay the foundation to probe for a causal relationship between one of the most well-studied human microbiota phenotypes and its associated disease with atomic resolution.

Because colibactin has been recalcitrant to isolation, knowledge of its structure and bioactivity derives from diverse interdisciplinary findings. Enzymology, bioinformatic analysis of the *clb* BGC, stable isotope feeding experiments, characterization of biosynthetic intermediates, and gene deletion and editing studies have given insights into many elements of colibactin's biosynthesis, bioactivity, and cellular trafficking (*11*–*15*). Consistent with the determination that *clb*$^+$ *E. coli* are genotoxic (*5*, *6*), a *clb* metabolite isolated from a mutant strain was shown to damage DNA in cell-free experiments (*16*). Subsequently, chemical synthesis was used to access other *clb* metabolites and putative biosynthetic intermediates and further a mechanistic model to explain colibactin's genotoxic properties (*17*).

Merging this data forms a picture, albeit incomplete, of colibactin's biosynthesis, structure, and mode of genotoxicity. Colibactin is assembled in a linear prodrug form referred to as precolibactin (Fig. 1, **1**). Key structural elements of precolibactins include a terminal *N*-myristoyl-D-Asn amide (Fig. 1, blue in **1**) (*18*–*20*) and an aminocyclopropane residue (Fig. 1, green in **1**) (*16*, *21*, *22*). The terminal amide is cleaved in the periplasm by a pathway-dedicated serine protease known as colibactin peptidase (ClbP) (*23*, *24*). The resulting amine **2** undergoes a series of cyclization reactions to generate spirocyclopropyldihydro-2-pyrrolone that resemble **3** (Fig. 1) (*17*, *25*). These cyclizations place the cyclopropane in conjugation with both an imine and amide, rendering the cyclopropane electrophilic and capable of alkylating DNA (a detailed mechanism of cyclization and DNA alkylation is provided in fig. S1) (*14*, *17*). The adenine adduct **4** was identified in the digestion mixture of linearized pUC19 DNA exposed to *clb*$^+$ *E. coli* (*26*) and in colonic epithelial cells of mice infected with *clb*$^+$ *E. coli* (Fig. 1) (*27*). However, a recent study established that *clb*$^+$ *E. coli* cross-link DNA (*28*), suggesting that colibactin contains a second DNA-reactive site that has yet to be elucidated. The full structure of colibactin and the site of the second alkylation have remained undefined.

Mutation of *clbP* has been widely used to promote the accumulation of precolibactins and facilitate isolation. Precolibactins A to C (**5** to **7**) and precolibactin 886 (**8a**) exemplify the metabolites produced in Δ*clbP* cultures (Fig. 1) (*16*, *20*, *22*, *29*–*32*). The persistence of the *N*-myristoyl-D-Asn residue (deriving from mutation of *clbP*) changes the fate of the linear precursor **1** and promotes pyridone formation (for **5** to **7**) (*14*, *17*) or macrocyclization (for **8**) (Fig. 1) (*33*). Precolibactin 886 (**8a**) is an advanced metabolite that requires every biosynthetic gene in the pathway except polyketide synthase (PKS) *clbO*, type II thioesterase *clbQ*, and amidase *clbL* (Fig. 1) (*25*). Recently, precolibactin 969 (Fig. 1, **8b**), which bears a terminal oxazole ring, was reported, but this product still does not account for every biosynthetic step encoded in the *clb* gene cluster (*34*). Genetic studies established that deletion of any biosynthetic gene in the *clb* locus abolishes cytopathic effects (*5*); thus, the full biosynthetic product is believed to possess additional chemical functionalities not contained in **8a** or **8b** (Fig. 1).

Characterization of colibactin-DNA cross-links and biosynthetic proposal

Because colibactin has proven recalcitrant to isolation, we focused on structural elucidation of the DNA cross-links generated by *clb*$^+$ *E. coli* (*28*). This approach circumvents the challenges in obtaining pure samples of the metabolite from fermentation extracts and instead relies intensively on mass spectrometry (MS) and tandem MS analysis [rather than conventional nuclear magnetic resonance (NMR) analysis]. The stereochemical assignments in the structures that follow are based on established intermediates and nonribosomal peptide synthetase (NRPS)–polyketide synthase (PKS) biosynthetic logic.

Tandem MS analysis of the digestion products of linearized pUC19 DNA that had been exposed to *clb*$^+$ *E. coli* was used to elucidate the structure of the adenine adduct, **4** (Fig. 1) (*26*). In that study, wild-type *E. coli* BW25113 and its cysteine and methionine auxotrophs (Δ*cysE* and Δ*metA*) (*35*) containing *clb* on a bacterial artificial chromosome (BAC) were used. The latter two cultures were supplemented with L-[U-^{13}C]-Cys or L-[U-^{13}C]-Met, which are known precursors to the thiazole (*16*) and aminocyclopropane (*16*, *21*, *36*) residues of colibactin, respectively. This approach allowed for the identification of

[1]Department of Chemistry, Yale University, New Haven, CT 06520, USA. [2]Chemical Biology Institute, Yale University, West Haven, CT 06516, USA. [3]Department of Microbial Pathogenesis, Yale School of Medicine, New Haven, CT 06536, USA. [4]Department of Molecular Biophysics and Biochemistry, Yale School of Medicine, New Haven, CT 06520, USA. [5]W. M. Keck Biotechnology Resource Laboratory, Yale School of Medicine, New Haven, CT 06510, USA. [6]Department of Pharmacology, Yale School of Medicine, New Haven, CT 06520, USA.

*These authors contributed equally to this work. †Present address: New York University Abu Dhabi, Post Office Box 129188, Abu Dhabi, United Arab Emirates. ‡Present address: Department of Process Research and Development, Merck, Rahway, NJ 07065, USA.

§Corresponding author. Email: jason.crawford@yale.edu (J.M.C.); seth.herzon@yale.edu (S.B.H.)

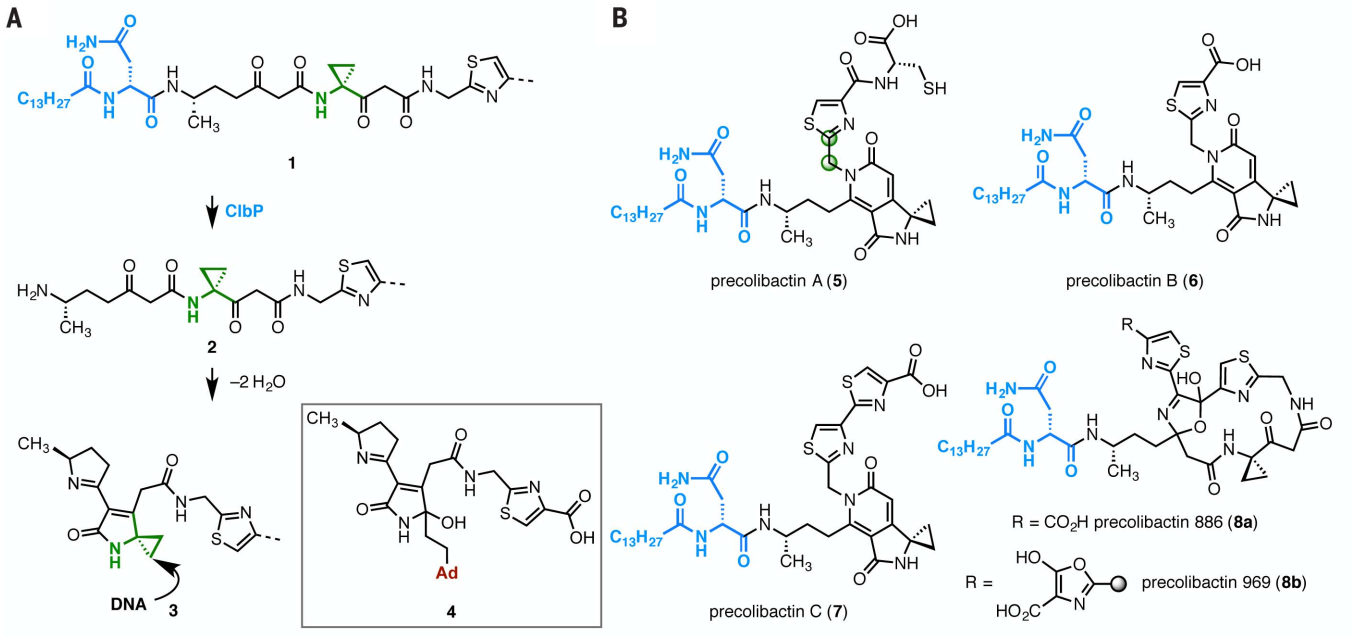

Fig. 1. Structures and reaction pathways of selected *clb* biosynthetic products. (**A**) Established mechanism of DNA mono-alkylation by *clb* metabolites formed in wild-type cultures. (**B**) Structures of *clb* metabolites formed in Δ*clbP clb*$^+$ *E. coli* cultures. The green spheres in structure **5** denote the carbon atoms derived from glycine.

clb metabolite–nucleobase adducts by mining for shifts in the mass spectra between unlabeled wild-type and labeled auxotrophic cultures.

Further analysis of this data revealed a compound of mass/charge ratio (m/z) = 537.1721 (z = 2) (Fig. 2A and supplementary materials), which corresponds to a molecular formula of $C_{47}H_{50}N_{18}O_9S_2^{2+}$ [error = 0.37 parts per million (ppm)]. The doubly charged ion (m/z = 537.1721) was shifted by three or four units in cultures containing L-[U-^{13}C]-Cys or L-[U-^{13}C]-Met, respectively, supporting the presence of two thiazole and two cyclopropane residues. To gain further insights into the structure, we analyzed its production in glycine (Δ*glyA*) and serine (Δ*serA*) auxotrophs. These cultures were supplemented with [U-^{13}C]-Gly, L-[U-^{13}C]-Ser, or L-[U-^{13}C, ^{15}N]-Ser. Glycine serves as the CN extension in the 2-methylamino thiazole of precolibactin A (Fig. 1, **5**, highlighted by green spheres) (*16*), whereas serine is incorporated into precolibactin 886 (**8a**) by means of an unusual α-aminomalonate extender unit (*31*, *32*, *37*). The doubly charged ion (m/z = 537.1721) was shifted by one unit in cultures containing [U-^{13}C]-Gly, indicating incorporation of one glycine building block. However, this ion was shifted by 1.5 units in cultures containing L-[U-^{13}C]-Ser and by two units in cultures containing L-[U-^{13}C, ^{15}N]-Ser, indicating that three carbon atoms and one nitrogen atom are derived from serine. This unexpectedly suggests that two α-aminomalonate building blocks are transformed into two distinct fragments that are incorporated into colibactin's structure, rather than only one, or two identical, serine-derived building blocks. These cultures also produced a range of higher-molecular-weight isotopologs owing to amino acid metabolism and incorporation into other building blocks.

When wild-type *clb*$^+$ *E. coli* cultures were grown in medium lacking amino acids and supplemented with D-[U-^{13}C]-glucose, the doubly charged ion (m/z = 537.1721) was shifted by 18.5 units, establishing that the colibactin residue contained 37 carbon atoms. Cultivation in minimal medium containing [^{15}N]-ammonium chloride shifted the doubly charged ion by four units, indicating that the colibactin residue contained eight nitrogen atoms. A double-labeling experiment by using D-[U-^{13}C]-glucose and [^{15}N] ammonium chloride resulted in a shift of 22.5 units, confirming the results of the individual labeling experiments. The singly charged (z = 1) and triply charged (z = 3) ions were also detected in many of these auxotrophs and provided data of comparable quality (supplementary materials). A fragment ion corresponding to protonated adenine was observed in the tandem MS of each of the isotopically labeled and unlabeled adducts. Additionally, the consecutive loss of two adenine bases was observed in all labeling experiments. Last, the doubly charged ion (m/z = 537.1721) was detected when the experiment was conducted with poly(AT) as the substrate. Collectively these data suggest the generation of a bis(adenine) adduct and a molecular formula of $C_{37}H_{38}N_8O_9S_2$ for the colibactin residue contained therein.

On the basis of these data, we reconsidered the unaccounted functions of ClbO, ClbQ, and ClbL (Fig. 3). ClbO is a PKS that accepts an α-aminomalonyl-extender unit in protein biochemical studies (*32*), suggesting a canonical extension step. ClbQ serves as an editing thioesterase and also off-loads intermediary structures, with an observed preference for hydrolyzing thioester intermediates toward the middle of the assembly line (*25*, *31*, *38*). Although these off-loaded structures enhance the metabolite diversity arising from the pathway, we reasoned that they could also serve as downstream substrates. In this scenario, off-loading of intermediate **A** (Fig. 3) followed by an uncharacterized ClbL-mediated amidase activity could promote a heterodimerization. The resulting structure would accommodate the isotopic labeling studies, including the presence of two aminocyclopropane units derived from methionine (Fig. 3) and the detection of double nucleobase adducts arising from twofold alkylation of DNA. While our work was under revision, a recent study supporting ClbL as an amidase was published (*39*, *40*).

Taking all of these data into consideration, we formulated the structure of the observed parent ion as the bis(adenine) adduct **9** (Fig. 2B). The experimental and theoretical masses for **9** are in agreement (error = 0.37 ppm). The positions of the cysteine, methionine, serine, and glycine isotopic labels depicted in **9**, which were determined with tandem MS analysis, are fully supported by all known elements of colibactin biosynthesis (supplementary materials). The tandem MS fragments **10** to **12** shown in Fig. 2C provide further robust support for the structure **9**. Each of the ions **10** to **12** possessed the expected mass shift in the individual labeling experiments (supplementary materials).

The structure **9** is fully supported by all published data in the field, to our knowledge (Fig. 2B). The bis(adenine) adduct **9** derives from twofold alkylation of DNA through cyclopropane

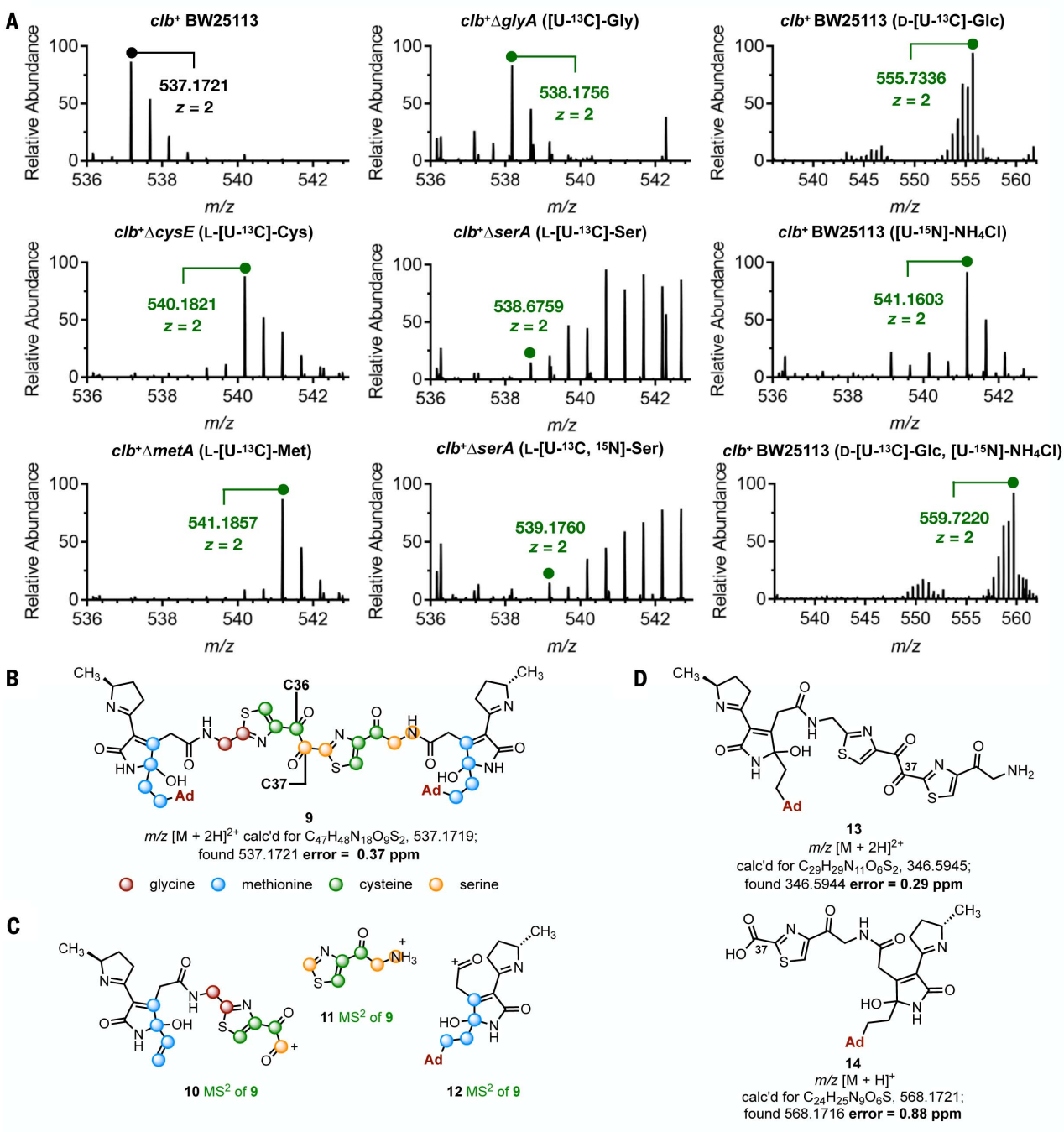

Fig. 2. Selected HRMS signals deriving from treatment of linearized pUC19 DNA with *clb*$^+$ *E. coli*, followed by digestion. (**A**) Natural abundance and stable isotope derivatives of **9**. The highest-intensity labeled peaks (green) were selected for analysis, except for Ser, which was extensively metabolized. All selected ions were confirmed by means of tandem MS. $[M+2H]^{2+}$ ions are marked. (**B**) Structure of the colibactin-bis (adenine) adduct **9**. (**C**) Structures of the daughter ions **10** to **12**. (**D**) The DNA adducts **13** and **14**.

ring-opening, which is in agreement with the discovery that colibactin derivatives containing one cyclopropane residue alkylate DNA by means of a parallel pathway (*17*). Additionally, twofold alkylation of DNA to form **9** is consistent with the observation that *clb*$^+$ *E. coli* cross-link DNA and activate cross-link repair machinery in human cells (*28*). The proposed ClbL-mediated transacylation appends the second (pro)warhead, and these data explain why *clbL* mutants alkylate but do not cross-link exogenous DNA (*41*). The aminal functional groups in **9** derive from aerobic oxidation of the ring-opened products, as previously established in studies of simpler colibactin derivatives (Fig. 2B) (*26*, *42*). Last, in agreement with the well-established propensity of α-diketones to hydrate under aqueous conditions [dissociation constant (K_d) for dissociation of the monohydrate of butane-2,3-dione = 0.30] (*43*), the product of hydration of C37 (**S1**) was also detected (supplementary materials). Tandem MS and isotopic labeling data for **S1** fully support the structure of the hydrate and are in agreement with the diketone form **9** (supplementary materials).

Additional nucleobase adducts were detected at discrete retention times (Fig. 2D). The methylaminoketone **13** and its corresponding hydrate

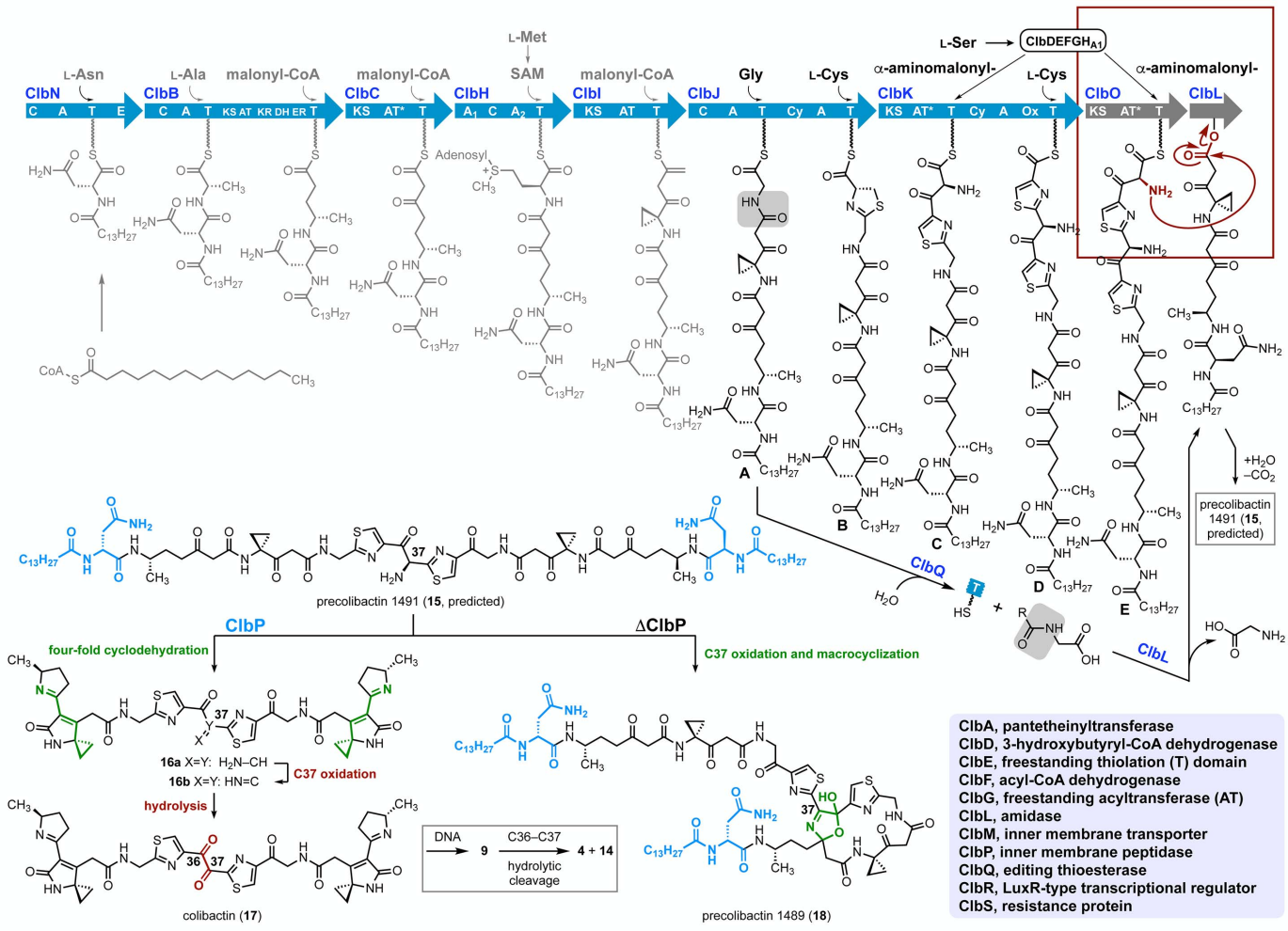

Fig. 3. Proposed biosynthesis of (pre)colibactin. The early stages in the biosynthetic pathway are grayed for clarity. The heterodimerization is highlighted in the red box (top right). Intermediates B to E are also possible substrates for thioesterase ClbQ, although promiscuous ClbQ has a known preference for hydrolyzing intermediates toward the middle of the assembly line. Amino acids are depicted at their sites of pathway entry. Domain abbreviations are C, condensation; A, adenylation; E, epimerization; KS, ketosynthase; KR, ketoreductase; DH, dehydratase; ER, enoylreductase; AT*, inactivated acyltransferase (AT); Cy, dual condensation/cyclization; and Ox, oxidase.

(**S15**) are of special importance (supplementary materials): These are likely formed by hydrolytic off-loading of the biosynthetic product **E** (Fig. 3); its enzyme precursor serves as the acceptor in the ClbL transacylation step we proposed. The known adduct **4** (Fig. 1A) (*26*, *27*) and the right-hand fragment **14** (Fig. 2D) were also detected (supplementary materials). Fragment **14** is important because we have demonstrated that the C36–C37 bond in advanced colibactins is susceptible to oxidative cleavage in the presence of weak nucleophiles, such as water or methanol (*33*). Hydrolytic degradation of **9** at this bond accounts for isolation of the earlier mono (adenine) adduct **4** (*26*, *27*) and, now, the right-hand fragment **14** (Fig. 2D). We also detected the hydrate and diketone of a full-length mono (adenine) adduct (**S2** and **S7**) (supplementary materials).

The cross-linking, digestion, and MS experiments performed above served to reveal the presence of the bis(adenine) adduct **9** and its corresponding hydrate **S1**. Although the relevance of these bis(nucleobase) adducts to colibactin genotoxicity remains to be determined, we sought to probe for their production in human tissue culture. Accordingly, HCT-116 colon cells were infected with *clb*$^+$ *E. coli* BW25113. After a 2-hour infection, the human cells were separated, and their genomic DNA was isolated, digested, and subjected to MS analysis. We were able to detect trace levels of the bis(adenine) adduct **9** (error = 1.49 ppm) and its corresponding hydrate **S1** (error = 0.37 ppm). The retention time of these materials were identical to the material derived from pUC19 DNA exposed to the *clb*$^+$ *E. coli* BW25113 (supplementary materials).

Identification of colibactin (17)

We then searched *clb*$^+$ *E. coli* cultures for the structures of the α-ketoamine **16a**, the corresponding α-ketoimine **16b**, and the α-dicarbonyl **17** (Fig. 3), which were anticipated on the basis of the structure of the bis(adenine) adduct **9** and established biosynthetic logic. Although our data do not allow us to exclude **16a** or **16b** as active *clb* genotoxic contributors (oxidation of **16a** and hydrolysis of **16b** lead to the observed α-dicarbonyl under our experimental conditions), our prior studies established that α-ketoamines and α-ketoimines structurally related to **16a** and **16b** rapidly transform to the corresponding α-dicarbonyl under mild conditions (*33*). Moreover, we were unable to detect **16a** or **16b** in freshly prepared *E. coli* extracts. However, the proton and sodium adducts of colibactin (**17**) were observed in *E. coli* DH10B harboring the *clb* BAC (supplementary materials). Colibactin (**17**) was not detectable in a *clbO* deletion mutant and a *clbL* active site point mutant (S179A, indicating serine at position 179 was replaced by alanine) (Fig. 4A). Because colibactin (**17**) was detected at low abundance, we also confirmed production in the wild-type probiotic *E. coli* Nissle 1917. Deletion of the *clb* genomic island (*20*) in Nissle 1917 or a *clb*$^-$ BAC control strain abolished production, as expected.

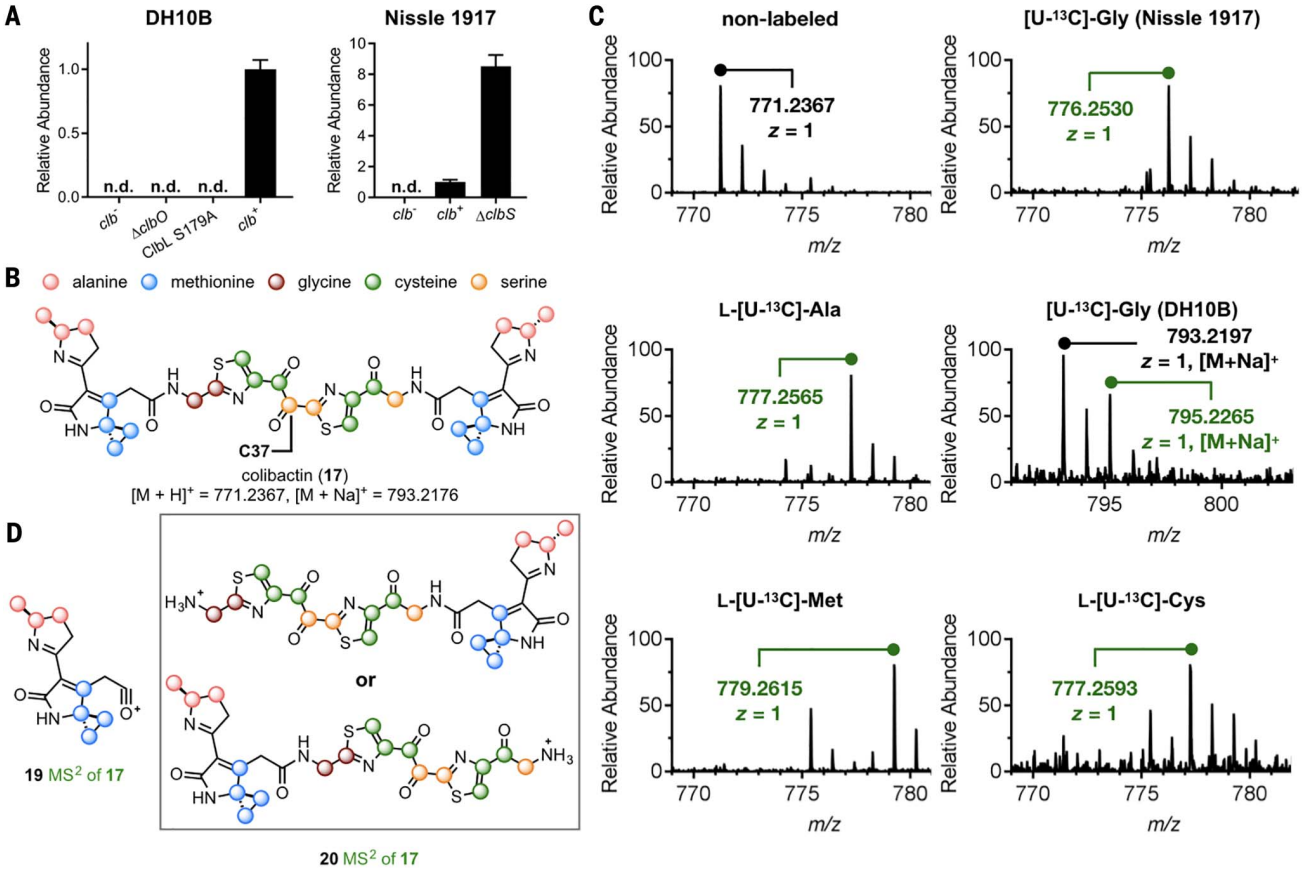

Fig. 4. Stimulation, genetic dependence, and isotopic labeling of natural colibactin (17). (**A**) Genetic dependence of colibactin (**17**) production in *clb*$^+$ DH10B and Nissle 1917. n = 3 biological replicates; error represents standard deviation. n.d., not detected. (**B**) Isotopic labeling pattern of colibactin (**17**). (**C**) Results of isotopic labeling studies of colibactin (**17**) in Nissle 1917 (Δ*clbS*). [U-^{13}C]-Gly labeling was conducted in both Nissle 1917 (Δ*clbS*), which also led to glycine-derived serine labeling, and *clb*$^+$ DH10B. The highest-intensity labeled peaks (green) were selected for analysis. $[M+H]^+$ ions are marked unless otherwise noted. (**D**) Ions observed in the tandem MS of colibactin (**17**). The two structures of ion **20** are equally plausible based on the MS data.

We hypothesized that the titer of colibactin (**17**) might be higher in a *clbS* Nissle 1917 mutant (*42*, *44*) because we previously established that ClbS is a self-resistance enzyme that catalyzes hydrolytic ring-opening of the cyclopropane ring (*42*). Although deletion of *clbS* leads to a fitness defect and activates a *clb*-dependent bacterial SOS DNA damage response (*44*), this genetic modification resulted in an 8.5-fold improvement in the signal intensity (Fig. 4A).

We then individually supplemented *E. coli* Nissle 1917 Δ*clbS* cultures with labeled amino acids. Colibactin (**17**) (Fig. 4, B and C) incorporated two equivalents of cysteine, methionine, and alanine, as expected on the basis of its proposed structure. The cultures labeled with L-[U-^{13}C]-Ser and [U-^{13}C]-Gly produced a range of isotopologs owing to their metabolism and incorporation into other building blocks (supplementary materials). To account for this variation, we used serine-derived enterobactin, an iron-scavenging siderophore in *E. coli*, as an internal control for comparison (fig. S118). We also repeated glycine labeling in *clb*$^+$ DH10B for confirmation of dominant mono-labeling of glycine in colibactin (**17**). The key tandem MS ions **19** and **20** were observed and provide further support for colibactin's structure (Fig. 4D). Because of the nearly C_2 symmetric structure of colibactin (**17**), the two structures of **20** shown are equally plausible according to the available data. Similar to the colibactin–DNA adducts, we observed the C37 hydrate of colibactin (**17**) (**S34**) (supplementary materials).

Characterization of precolibactin 1489 (18)

Every biosynthetic enzyme encoded in the *clb* gene cluster is necessary to observe the genotoxic phenotype associated with *clb*$^+$ *E. coli* (*5*). Although truncated precolibactins such as precolibactin 886 (Fig. 1B, **8a**) can be detected as macrocyclization products in nongenotoxic *clbP* peptidase mutants (*31*), precolibactin 886 (**8a**) is still produced in mutants of *clbL*, *clbO*, and *clbQ* in a *clbP*-deficient genetic background (ClbP S95A active site point mutant) (*25*). Additionally, the recently characterized metabolite precolibactin 969 (**8b**), isolated from a *clbP*/*clbQ*/*clbS* triple mutant (*34*), does not account for *clbL* and *clbQ* and was undetectable in freshly prepared organic extracts of a *clbP*-deficient strain under our experimental conditions. Given the structure of colibactin (**17**) and the requirement of every biosynthetic enzyme for cytopathic effects (*5*), we reasoned that more complex precolibactins existed.

Accordingly, we searched for the precolibactin that could account for colibactin (**17**) in *clb*$^+$ DH10B (ClbP S95A) (*25*). Although we were not able to detect the expected unstable linear precursor precolibactin 1491 (Fig. 3, **15**) or its oxidation products, we detected both the proton and sodium ion adducts of a metabolite predicted to be the macrocycle precolibactin 1489 (**18**) (supplementary materials). We used genome editing to individually inactivate the catalytic domains from ClbH to ClbL in the biosynthetic pathway (*25*). Precolibactin 1489 (**18**) was genetically dependent on all of the enzymatic steps in the pathway (Fig. 5A). Production was only detected in an acyltransferase (AT) domain mutant of ClbI; metabolites dependent on this single domain can be complemented in trans by other ATs in the cell (*25*). Thus, precolibactin 1489 (**18**) represents the first reported product derived from the complete *clb* biosynthetic pathway. A

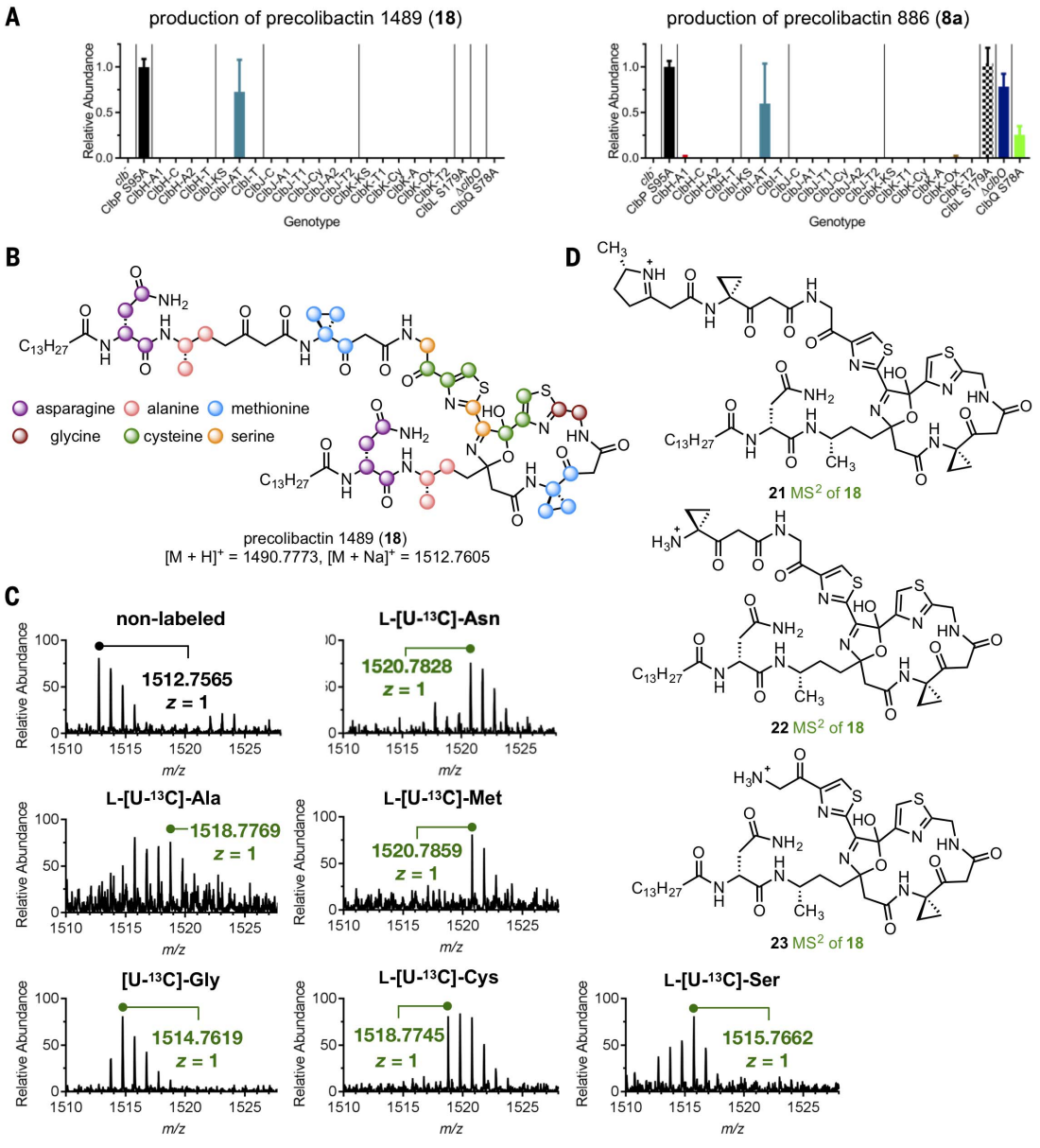

Fig. 5. Genetic, tandem MS, and isotopic labeling support for precolibactin 1489 (18). (**A**) Precolibactin 1489 (**18**) biosynthesis requires all biosynthetic enzymes in the *clb* gene cluster. Precolibactin 886 (**8a**) is still produced in *clbL*, *clbO*, or *clbQ* mutants. $n = 5$ biological replicates; error represents standard deviation. (**B**) Position of isotopic labels in precolibactin 1489 (**18**), as established by means of tandem MS analysis. (**C**) Isotopic labeling studies of precolibactin 1489 (**18**) in a *clb*$^+$ DH10B strain deficient in ClbP catalytic activity. (**D**) Proposed structures of ions **21** to **23** (fig. S125C) derived from the tandem MS of precolibactin 1489 (**18**).

similar analysis confirmed that precolibactin 886 (**8a**) was still produced in *clbL*, *clbO*, or *clbQ* mutants.

The structure of precolibactin 1489 (**18**) is supported by extensive ^{13}C-isotopic amino acid labeling and tandem MS analysis (Fig. 5, B to D, and fig. S125). Labeled methionine, glycine, alanine, cysteine, and serine precursors incorporated into precolibactin 1489 (**18**) in a manner fully consistent with its biosynthesis and proposed structure. Additionally, two units of L-[U-^{13}C]-Asn were incorporated, supporting the presence of two *N*-myristoyl-D-Asn residues, as expected. Tandem MS analysis of precolibactin 1489 (**18**) produced the ions **21** to **23** and **S35** to **S37**, which are also consistent with the proposed structure (Fig. 5D and fig. S125C). On the basis of the recent determination that ClbP-deacylation of precolibactin 886 (**8a**) produces a nongenotoxic pyridone (*33*), it seems likely that precolibactin 1489 (**18**) is simply a stable product arising from oxidation and macrocyclization of the putative linear precursor precolibactin 1491 (Fig. 3, **15**). Regardless, these studies support a twofold *N*-acyl-D-Asn prodrug activation mechanism, in which ClbP peptidase sequentially initiates the formation of two electrophilic architectures.

Confirmation of the structure of colibactin (17)

The structure of colibactin (**17**) was confirmed with chemical synthesis. The presence of two electrophilic spirocyclopropyldihydro-2-pyrrolone (*17*) and the hydrolytically labile C36–C37 α-dicarbonyl (*33*) necessitated a careful analysis of potential synthetic pathways. The essential elements of our strategy are outlined in Fig. 6A. Whereas in earlier studies (*17*), monomeric colibactins were assembled by a linear approach [stepwise formation of bonds a, b, and c, in that order (Fig. 6A)], we recognized that colibactin (**17**) could be assembled through a twofold coupling (a, a′ bond formation) of the diamine **26** with the β-ketothioester **25** (Fig. 6A). In addition to increased convergence, this approach masks the reactive (*17*) spirocyclopropyldihydro-2-pyrrolone as identical stable vinylogous imides. We have established that *N*-deacylation followed by mild neutralization is sufficient to induce cyclization and formation of the spirocyclopropyldihydro-2-pyrrolone residues (*17*, *41*). On the basis of our observations that C36–C37 α-aminoketones undergo spontaneous oxidation (*33*), we targeted an α-hydroxyketone in place of the α-dicarbonyl in colibactin (**17**). This was projected to allow for the assembly of **26** by means of benzoin addition, followed by late-stage oxidation to

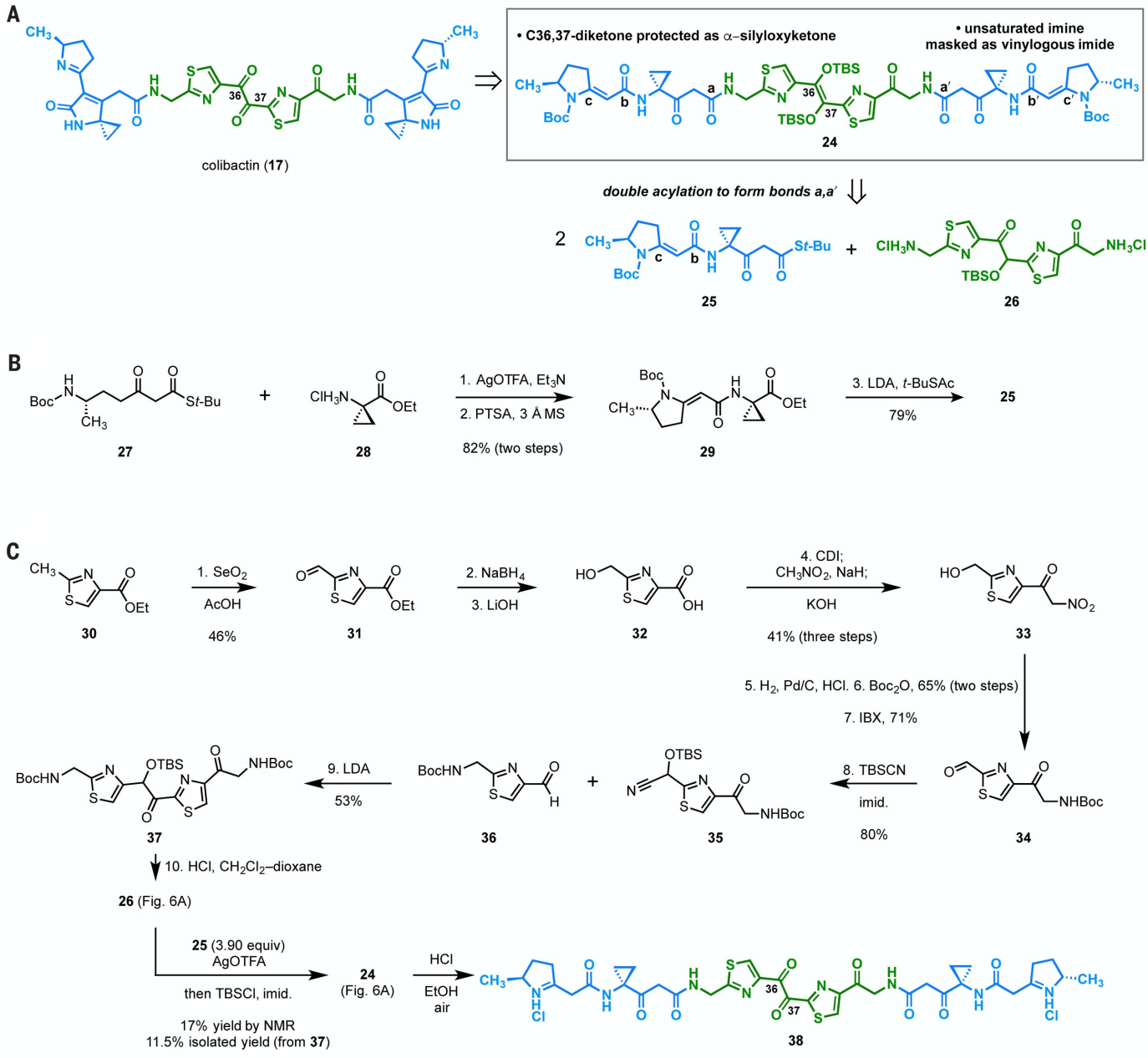

Fig. 6. Synthesis of the colibactin precursor 38. (**A**) Retrosynthetic analysis of colibactin (**17**). (**B**) Synthesis of the β-ketoester **25**. (**C**) Synthesis of the α-silyloxyketone **26** and the linear precursors **24** and **38**.

generate the sensitive α-dicarbonyl. In our synthesis of precolibactin 886 (Fig. 1B, **8a**) (*33*), the initial ketone was generated at C36. However, in exploratory experiments, we found that intermediates with a C37 ketone were more stable and pursued these.

The synthesis of the β-ketothioester **25** is shown in Fig. 6B. Silver trifluoroacetate–mediated coupling of the known β-ketothioester **27** (*17*) with ethyl 1-aminocyclopropyl-1-carboxylate (**28**) generated a β-ketoamide that was cyclized to the vinylogous imide **29**. Addition of the lithium enolate of *tert*-butyl thioacetate to **29** then provided the β-ketothioester **25**. The diamine **26** was synthesized by means of the route shown in Fig. 6C. Selenium dioxide oxidation of the commercial reagent ethyl 2-methylthiazole-4-carboxylate (**30**) generated the aldehyde **31** (Fig. 6C). Reduction of the aldehyde, followed by saponification of the ester, provided the hydroxy acid **32** (Fig. 6C). Treatment of the hydroxy acid **32** with excess 1,1′-carbonyldiimidazole (CDI) resulted in acylation of the primary alcohol and activation of the carboxylic acid as the expected acyl imidazole [liquid chromatography–MS (LC-MS) analysis]. Addition of sodium nitromethanide, followed by in situ hydrolysis of the acylated alcohol, formed the α-nitroketone **33** (Fig. 6C). Hydrogenolysis of the nitro group, followed by protection of the resulting primary amine and oxidation of the primary alcohol [2-iodoxybenzoic acid (IBX)], provided the aldehyde **34** (Fig. 6C). Silyl cyanohydrin formation, deprotonation, and addition of the aldehyde **36** (*33*) generated the α-silyloxy ketone **37** (Fig. 6C). The carbamate protecting groups were removed under acidic conditions to furnish the diammonium salt **26** (Fig. 6A).

Silver-mediated coupling of the diamine **26** with an excess of the β-ketothioester **25** provided the expected twofold coupling product (LC-MS analysis). However, all attempts to purify

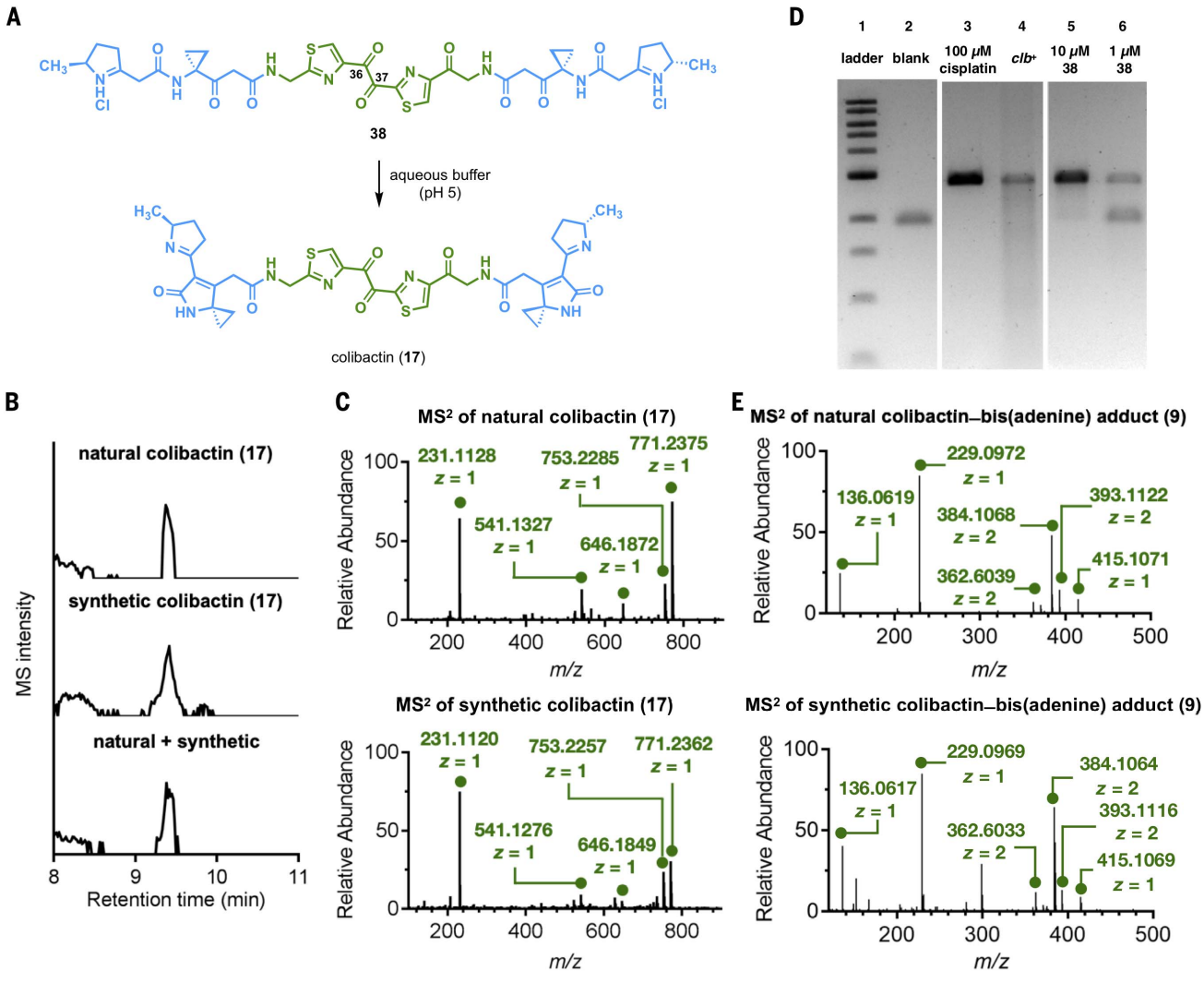

Fig. 7. Confirmation of the predicted structure of colibactin (17). (**A**) Cyclization of intermediate **38** to colibactin (**17**). (**B**) LC-MS coinjection analysis of colibactin (**17**): natural (top), synthetic (middle), and coinjection (bottom). (**C**) Tandem MS data of natural colibactin (**17**, top) and synthetic colibactin (**17**, bottom). Collision energy = 30 eV. Additional data is available in fig. S127. (**D**) DNA cross-linking assay by using linearized pUC19 DNA and synthetic intermediate **38**. (**E**) Tandem MS data of the bis(adenine) adduct **9** derived from natural and synthetic colibactin (**17**).

this product resulted in extensive decomposition deriving from cleavage of the C36–C37 bond (LC-MS analysis). To circumvent this, we developed conditions to protect this residue in situ. Thus, immediately after the fragment coupling, the enedisilyl ether **24** was formed through silylation of the product mixture (Fig. 6A). The stereochemistry of the central alkene was determined to be (*E*), as shown, by means of two-dimensional rotating-frame nuclear Overhauser effect correlation spectroscopy (2D-ROESY) analysis. The yield of this twofold coupling-protection sequence was 17% (based on ^{1}H NMR analysis of the unpurified product mixture, using an internal standard), and **24** was isolated in 11.5% yield after reverse-phase high-performance LC (HPLC) purification. By this approach, 5- to 7-mg batches of **24** were readily prepared.

Conversion of the protected intermediate **24** to colibactin (**17**) proved to be challenging because we found that introduction of the C36–C37 α-dicarbonyl rendered the intermediates exceedingly unstable. This is consistent with an earlier model study (*33*) that demonstrated rupture of the C36–C37 bond under slightly basic conditions. Ultimately, we found that treatment with concentrated hydrochloric acid in ethanol resulted in instantaneous cleavage of the carbamate-protecting groups and one silyl ether; this was followed by slower and sequential cleavage of the remaining silyl ether and aerobic oxidation to the α-dicarbonyl **38**. The α-dicarbonyl **38** was accompanied by variable amounts of the diketone hydrate (LC-MS analysis) (fig. S127 and table S70), as observed for the bis(adenine) adduct **9** and colibactin (**17**).

On dissolving **38** in rigorously deoxygenated aqueous citric acid buffer (pH = 5.0), we observed double cyclodehydration to form colibactin (**17**) (Fig. 7A). This mild cyclization is consistent with earlier studies that established that synthetic iminium ions resembling **38** cyclize to spirocyclopropyldihydro-2-pyrrolone genotoxins instantaneously under aqueous conditions (*17*, *41*) and genetic studies that support the off-loading of linear biosynthetic intermediates, followed by spontaneous transformation to the unsaturated imine electrophile (*25*). Although we were unable to separate small amounts of side products deriving from hydrolytic ring-opening of the vinylogous urea of **38**, synthetic colibactin (**17**) obtained in this way was indistinguishable from natural material by means of LC-MS coinjection and tandem MS analysis by using a range of collision energies (20 to 50 eV) (Fig. 7, B and C, and fig. S127).

Although we could enhance mass spectral detection of natural colibactin (**17**) in the *clbS* mutant of Nissle 1917, the titers remained too low to facilitate isolation. Consequently, we turned to functional analysis of synthetic colibactin (**17**) in the DNA cross-linking assay to further confirm the structural assignment. We observed dose-dependent cross-linking of DNA (Fig. 7D)

by forming colibactin (**17**) in situ from the iminium diion **38** at pH 5 in the presence of DNA. Additionally, the DNA cross-links induced by synthetic colibactin (**17**) were indistinguishable from those produced by *clb*$^+$ *E. coli* (figs. S129 to S132) under basic denaturing gel conditions. Cross-linking was strongest at pH 5.0 and diminished as the pH was increased—an observation consistent with the known instability of the α-diketone under basic conditions (*33*). This was also consistent with the stability of the cross-links derived from *clb*$^+$ bacteria (supplementary materials). The DNA cross-links derived from **38** were isolated, digested, and subjected to tandem MS by using the same parameters used to analyze the natural colibactin–bis(adenine) adduct, which confirmed the assignment (Fig. 7E). All of the ions detected from cross-linking products derived from *clb*$^+$ *E. coli* BW25113 were detected by using synthetic **38** (supplementary materials). Collectively, the abundance of genetics data as well as these synthetic efforts confirm the structure of the major colibactin as **17**.

Conclusion

Elucidating the complete structure of colibactin (**17**) puts to rest the decade-long debate over the structure of the metastable metabolite. Correlative relationships abound in the microbiome field, but causative relationships are far more rare, primarily owing to a lack of detailed, molecular-level structure-function analysis. The development of a chemical synthesis of colibactin (**17**) enables researchers to probe for a causative relationship between the metabolite and CRC formation. The interdisciplinary approach we developed to determine and confirm colibactin's structure may be extensible to other low-abundance bioactive metabolites from complex backgrounds such as the human microbiome.

Materials and methods

NMR spectroscopy

Proton NMR spectra (^{1}H NMR) were recorded at 400, 500, or 600 MHz at 24°C, unless otherwise noted. Chemical shifts are expressed in parts per million (δ scale) downfield from tetramethylsilane and are referenced to residual protium in the NMR solvent ($CDCl_3$, δ 7.26; CD_2HOD, δ 3.31; $CDHCl_2$, δ 5.33; C_2D_5HSO, δ 2.50). Data are represented as follows: chemical shift, multiplicity (s, singlet; d, doublet; t, triplet; q, quartet; m, multiplet and/or multiple resonances; br, broad; app, apparent), coupling constant in Hertz, integration, and assignment. Proton-decoupled carbon NMR spectra (^{13}C NMR) were recorded at 100, 125, or 150 MHz at 24°C, unless otherwise noted. Chemical shifts are expressed in parts per million (δ scale) downfield from tetramethylsilane and are referenced to the carbon resonances of the solvent ($CDCl_3$, δ 77.17; CD_3OD, δ 49.0; CD_2Cl_2, δ 54.0; C_2D_6SO, δ 39.5). Signals of protons and carbons were assigned, as far as possible, by using the following two-dimensional NMR spectroscopy techniques: [^{1}H, ^{1}H] COSY (correlation spectroscopy), [^{1}H, ^{13}C] HSQC (heteronuclear single quantum coherence) and long range [^{1}H, ^{13}C] HMBC (heteronuclear multiple bond connectivity).

Infrared spectroscopy

Attenuated total reflectance Fourier transform infrared (ATR-FTIR) spectra were obtained using a Thermo Electron Corporation Nicolet 6700 FTIR spectrometer referenced to a polystyrene standard. Data are represented as follows: frequency of absorption (cm^{-1}), intensity of absorption (s, strong; m, medium; w, weak; br, broad).

Analytical LC-MS for synthetic chemistry

Analytical ultra high-performance liquid chromatography–MS (UPLC-MS) was performed on a Waters UPLC-MS instrument equipped with a reverse-phase C_{18} column (1.7 μm particle size, 2.1 by 50 mm), dual atmospheric pressure chemical ionization (API)/electrospray (ESI) MS detector, and photodiode array detector. Samples were eluted with a linear gradient of 5% acetonitrile–water containing 0.1% formic acid→100% acetonitrile containing 0.1% formic acid over 0.75 min, followed by 100% acetonitrile containing 0.1% formic acid for 0.75 min, at a flow rate of 800 μL/min.

HRMS for synthetic intermediates

High-resolution MS (HRMS) spectra were obtained on either a Waters UPLC-HRMS instrument equipped with a dual API/ESI high-resolution MS detector and photodiode array detector eluting over a reverse-phase C_{18} column (1.7 μm particle size, 2.1 by 50 mm) with a linear gradient of 5% acetonitrile–water containing 0.1% formic acid→95% acetonitrile–water containing 0.1% formic acid for 1 min, at a flow rate of 600 μL/min or an Agilent 6550A QTOF Hi Res LC-MS equipped with a 1290 dual spray API source eluting over an Agilent Eclipse Plus C_{18} column (1.7μm particle size, 4.5 by 50 mm) with a linear gradient of 5% acetonitrile–water containing 0.1% formic acid→95% acetonitrile–water containing 0.1% formic acid for 6 min, at a flow rate of 500 μL/min.

HRMS for natural (pre)colibactins

HRMS and tandem MS data were acquired by an Agilent iFunnel 6550 quadrupole time-of-flight (QTOF) mass spectrometer coupled to an Agilent Infinity 1290 HPLC, scanning from *m/z* 25–1700 and a Phenomenex Kinetex 1.7 μ C18 100 Å column (100 × 2.1 mm, flow rate 0.3 mL/min, a water–acetonitrile gradient solvent system containing 0.1% formic acid: 0 to 2 min, 5% acetonitrile; 2 to 26 min, 5 to 98% acetonitrile; hold for 10 min, 98% acetonitrile). The domain-targeted metabolomics result for precolibactin 1489 (**18**) was obtained by reanalyzing data from our previous study (*25*).

HPLC enrichment for natural colibactin-nucleobase adducts detected from the genomic DNA

For colibactin-mono(adenine) adduct

The digested mixture was dissolved in 100 μL of water and injected onto a semipreparative reverse phase HPLC system equipped with a Phenomenex Luna C8 (2) 100 Å column [250 × 10 mm, flow rate 4.0 mL/min, a gradient elution from 5 to 100% aqueous acetonitrile with 0.01% trifluoroacetic acid over 30 min (0 to 5 min, 5%; 5 to 30 min, 5 to 100%)] using a 1 min fraction collection window. Fractions 11 to 20 were combined, dried, and dissolved in 20 μL of methanol for further LC-MS anlalysis.

For colibactin-bis(adenine) adduct

The digested mixture was dissolved in 10 mL of water and injected onto a preparative reverse phase HPLC system equipped with Agilent Polaris C18-A 5 μm column [21.2 by 250 mm, flow rate 8.0 mL/min, a gradient elution from 5 to 100% aqueous acetonitrile with 0.01% trifluoroacetic acid over 30 min (0 to 5 min, 5%; 5 to 30 min, 5 to 100%)] using a 1 min fraction collection window. Fractions 21–30 were combined, dried, and dissolved in 20 μL of methanol for further LC-MS anlalysis.

HRMS (for natural colibactin–nucleobase adducts)

HRMS and tandem MS data were obtained at the Mass Spectrometry and Proteomics Resource of the W.M. Keck Foundation Biotechnology Resource Laboratory at Yale University (New Haven, CT). All HRMS/MS samples were prepared in 1-mL screw neck total recovery vials (Waters, Milford, MA). The concentration of the digested nucleosides was adjusted to 50 ng/μL before injection. 5 μL of sample was injected at 4°C. UPLC analysis was performed on an AcQuity M-Class Peptide BEH C18 column (130 Å pore size, 1.7 μm particle size, 75 μm by 250 mm) equipped with an M-Class Symmetry C18 trap column (100 Å pore size, 5 μm particle size, 180 μm by 20 mm) at 37°C. Trapping was initiated at 5 μL/min at 99.5% of aqueous mobile phase (0.1% formic acid in water) for 3 min, and the gradient for separation began at 3% organic mobile phase (0.1% formic acid in acetonitrile), and increased to 5% over 1 min, 25% over 32 min, 50% over 5 min, 90% over 5 min and then maintained at 90% for 5 min and then 3% over 2 min, and equilibrated for an additional 20 min. MS was acquired on an Orbitrap Elite FTMS (Thermo Scientific) or on an Orbitrap Fusion FTMS (Thermo Scientific). The Orbitrap Elite FTMS (Thermo Scientific) was set at full scan from *m/z* = 150 to 1800 at a resolution ranging from 30,000 to 60,000, and the data-dependent MS^2 scans were collected with collision induced dissociation (CID) at collision energies ranging from 35 eV to 40 eV. The Orbitrap Fusion FTMS (Thermo Scientific) was set to scan from *m/z* = 150 to 1100 with a resolution of 60,000, and the data-dependent MS^2 scans were collected with higher-energy collisional dissociation (HCD) at 32 eV collision energy using quadrupole isolation. The HRMS parameter was slightly modified for detecting colibactin-nucleobase adducts from the genomic samples. For mono(adenine) adduct, targeted single ion monitor (t-SIM) data-dependent MS^2 scan was applied. Four defined MS were

scanned: 540.1772, 568.1721, 537.1719, and 546.1772. Isolation window was set to 3 *m/z*, and the resolution was set to 120,000. Automatic gain control (AGC) target was set 5.0×10^4, and the maximum ion injection time was set as 100 ms. The signal threshold for the data-dependent MS^2 was set to 1.0×10^6, but no targeted MS^2 was detected owing to low signal. For the bis(adenine) adduct, the mass range of Orbitrap Fusion FTMS (Thermo Scientific) full scan was set as *m/z* = 510 to 590 with a resolution of 60,000. AGC target was set as 1.0×10^4 with maximum injection time set as 50 ms. Data was analyzed using the Thermo Xcalibur Qual Browser software (version 2.2).

Cell lines

E. coli strains include the *E. coli* K-12 BW25113 parent strain and its single gene knock-out strains: cysteine auxotroph JW3582-2 (Δ*cysE720::kan*), methionine auxotroph JW3973-1 (Δ*metA780::kan*), serine auxotroph JW2880-1 (Δ*serA764::kan*), and glycine auxotroph JW2535-2 (Δ*glyA725::kan*). The isolated BAC DNA (pBAC *clb*$^+$ and *clb*$^-$) were separately transformed into these BW25113-derived strains.

Mutant strains

E. coli Nissle 1917 Δ*clbS* was constructed as previously described (*20*). Briefly, the FRT-flanked spectinomycin resistance cassette of pIJ778 was amplified using primers with short sequence extensions homologous to the flanking regions of *clbS*. Purified polymerase chain reaction (PCR) products were desalted and transformed into *E. coli* Nissle 1917 carrying the lambda red recombinase system on plasmid pKD46. Transformants were selected by plating on streptomycin (50 μg/mL). Colonies were analyzed with overspanning PCR and the resulting product was sequenced to confirm the replacement of gene *clbS* with the spectinomycin resistance gene.

The DH10B Δ*clbO* strain was generated in a wild-type *clb*$^+$ BAC background (containing a functional copy of the colibactin peptidase, ClbP), as previously described (*25*). This full gene-deletion was generated in the same manner as above using the lambda red recombinase system, but with apramycin as the selection marker. To avoid potential polar effects on the pathway, recombineering plasmid pKD46 was cured and plasmid pCP20 encoding the FLP recombinase was introduced in order to flip out the apramycin gene cassette. Successful deletion was confirmed by overspanning PCR. The DH10B Δ*clbL*-S179A strain was generated in a wildtype background (functional copy of the colibactin peptidase, ClbP), as previously described (*25*). Briefly, multiplex automated genome engineering (MAGE) was used to insert a single codon mutation into an active site serine residue of *clbL*, as determined by homology alignments to characterized amidase domains. Multiplex allele-specific colony PCR (MASC-PCR) was used to screen for mutations introduced and verified through overspanning PCR of the gene of interest and subsequent sequencing.

DNA and nucleic acids

The 2686 bp plasmid pUC19 was purchased from New England Biolabs and linearized with the endonuclease EcoRI (New England Biolabs, 5 U/μg DNA). The linearized plasmid was purified using the Monarch® PCR and DNA Cleanup Kit (New England Biolabs) and eluted with 10 mM Tris–1 mM EDTA pH 8.0 buffer.

Preparation of media

Isotopically-labeled reagents were purchased from Cambridge Isotope Laboratories, including L-[U-^{13}C]-asparagine: H_2O ([$^{13}C_4$]-Asn, 99% ^{13}C), L-[U-^{13}C]-alanine ([$^{13}C_3$]-Ala, 99% ^{13}C), L-[U-^{13}C]-cysteine ([$^{13}C_3$]-Cys, 99% ^{13}C), L-[U-^{13}C]-methionine ([$^{13}C_5$]-Met, 99% ^{13}C), L-[U-^{13}C]-serine ([$^{13}C_3$]-Ser, 99%^{13}C), L-[U-^{13}C, ^{15}N]-serine ([$^{13}C_3$, ^{15}N]-Ser, 99% ^{13}C, 99%^{15}N), [U-^{13}C]-glycine ([$^{13}C_2$]-Gly, 99% ^{13}C), D-[U-^{13}C]-glucose ([$^{13}C_6$]-Glc, 99% ^{13}C), and [^{15}N]-ammonium chloride ($^{15}NH_4Cl$, 99% ^{15}N). To prepare the media for isolating partially labeled colibactin–nucleobase adducts, the labeled amino acids were separately incorporated into modified M9–casamino acid (CA) medium for culturing the corresponding auxotrophs including JW3582-2 (cysteine), JW3973-1 (methionine), JW2880-1 (serine), and JW2535-2 (glycine). Natural abundance cysteine, methionine, serine, and glycine were incorporated into modified M9-CA medium for culturing the BW25113 parent strain as a control. To prepare the modified M9-CA medium, the M9 minimal medium (Sigma) was supplemented with 0.4% glucose, 2 mM $MgSO_4$, 0.1 mM $CaCl_2$, chloramphenicol (12.5 μg/mL), and the following L-amino acid mass composition (5 g/L total): 3.5% Arg, 20.0% Glu, 2.5% His, 5.0% Ile, 8.0% Leu, 7.0% Lys, 4.5% Phe, 9.5% Pro, 4.0% Thr, 1.0% Trp, 6.0% Tyr, 5% Val, 4% Asn, 4% Ala, 4% Met, 4% Gly, 4% Cys, and 4% Ser. To prepare the media for isolating universally-labeled colibactin–nucleobase adducts, [$^{13}C_6$]-Glc, [^{15}N]-ammonium chloride, and a combination of [$^{13}C_6$]-Glc and [^{15}N]-ammonium chloride were separately incorporated into modified M9-glucose medium for culturing the BW25113 parent strain. Natural abundance glucose and ammonium chloride salt were incorporated into the modified M9-glucose medium for culturing the BW25113 parent strain as a control. The modified M9-glucose medium contained 6.78 g/L Na_2HPO_4, 3 g/L KH_2PO_4, 1 g/L NH_4Cl, and 0.5 g/L NaCl, and was supplemented with 0.4% glucose, 2 mM $MgSO_4$, 0.1 mM $CaCl_2$, and chloramphenicol (12.5 μg/mL). All amino acids were excluded from this medium. For detection of colibactin (**17**) and the hydrate **S34** from *E. coli* Nissle 1917 Δ*clbS* strain, the modified M9-CA medium was prepared with Difco M9 minimal medium powder (10.5 g/L), 0.4% glucose, 2 mM $MgSO_4$, 0.1 mM $CaCl_2$, spectinomycin (100 μg/mL), and the following L-amino acid mass composition (5 g/L total): 3.5% Arg, 20.0% Glu, 2.5% His, 5.0% Ile, 8.0% Leu, 7.0% Lys, 4.5% Phe, 9.5% Pro, 4.0% Thr, 1.0% Trp, 6.0% Tyr, 5% Val, 4% Asn, 4% Ala, 4% Met, 4% Gly, 4% Cys, and 4% Ser. D-[U-^{13}C]-amino acids were supplemented instead of normal amino acids for isotopic labeling experiments. For detection of precolibactin 1489 (**18**) from the *E. coli* DH10B Δ*clbP* S95A strain, the same media compositions were used as for colibactin (**17**) and **S34** described above with a different antibiotic, chloramphenicol (12.5 μg/mL).

Preparation of DNA cross-links from natural colibactin

For each DNA cross-link preparation derived from the BW25113 parent strain, the JW3582-2 cysteine auxotroph, and the JW3973-1 methionine auxotroph, 3200 ng of linearized plasmid DNA was added to 800 μL of modified M9-CA media (containing the appropriate isotopically-labeled amino acid for each auxotroph) and then inoculated with 2.4×10^7 bacteria growing in exponential phase. The DNA–bacteria mixture was incubated for 4.5 hours at 37°C before isolation of the DNA. For each DNA cross-link preparation derived from the JW2880-1 serine auxotroph, 1000 ng of linearized plasmid DNA was added to 250 μL of modified M9-CA media containing either L-[U-^{13}C]-serine or L-[U-^{13}C, ^{15}N]-serine inoculated with 9.0×10^6 bacteria growing in exponential phase. The DNA–bacteria mixture was incubated for a total of 4.5 hours at 37°C before isolation of the DNA. During the incubation, 0.1 μg of appropriately labeled serine was added to the growing culture separately 1 hour and 3 hours after the initial inoculation. Each preparation was repeated in triplicate to accumulate sufficient DNA sample for analysis. For each DNA cross-link derived from the JW2535-2 glycine auxotroph, 1000 ng of linearized plasmid DNA was added to 250 μL of modified M9 minimal medium containing [U-^{13}C]-glycine inoculated with 3.2×10^7 bacteria growing in exponential phase. The final O.D. was adjusted to 0.2. The DNA–bacteria mixture was incubated for a total of 5 hours at 37°C before isolation of the DNA. For each universally labeled DNA cross-link, 1000 ng of linearized plasmid DNA was added to 250 μL of modified M9-glucose media containing D-[U-^{13}C]-glucose, or ^{15}N-ammonium chloride, or a combination of D-[U-^{13}C]-Glc and [^{15}N]-ammonium chloride. Each mixture was separately inoculated with 2.5×10^7 *clb*$^+$ BW25113 parent strain bacteria growing in exponential phase. The DNA–bacteria mixture was incubated for a total of 7 hours at 37°C before isolation of the DNA. To isolate the DNA from the cultures, the bacteria were pelleted by centrifugation. The DNA was isolated from the supernatant using the Monarch® PCR and DNA Cleanup Kit (New England Biolabs) and eluted using ultra purified water (Invitrogen). The isolated DNA was stored at −20°C until further use. To verify the presence of a DNA cross-link, a small quantity of DNA was analyzed by denaturing electrophoresis. To prepare the positive control for cross-linked DNA, 200 ng of linearized pUC19 DNA was treated with 100 μM of cisplatin (Biovision) in 10 mM sodium citrate pH 5 buffer with 5% final dimethyl sulfoxide (DMSO) concentration. Cross-linking with cisplatin (generates both intrastrand and interstrand cross-links) was conducted for 3 hours at 37°C.

Denaturing gel electrophoresis

The concentration of each DNA sample was adjusted to 10 ng/μL using water. 5 μL (50 ng) of the DNA sample was removed and mixed with 15 μL of 0.4% denaturing buffer (0.53% sodium hydroxide, 10% glycerol, 0.013% bromophenol blue) or 1% denaturing buffer (1.33% sodium hydroxide, 10% glycerol, 0.013% bromophenol blue). The DNA was denatured for 10 min at 4°C and then immediately loaded onto a 1% agarose Tris Borate EDTA (TBE) gel. The samples were run in TBE buffer for 1.5 hours at 90 V. The DNA was visualized by staining with Sybr® Gold (Thermo Fisher) for 2 hours.

Digestion of clb$^+$ cross-linked DNA

Following gel verification of the DNA cross-link, 2000 ng of the remaining DNA was digested using the Nucleoside Digestion Mix (New England Biolabs) for 1 hour at 37°C. The digested DNA was stored at −80°C prior to MS analysis.

Preparation of *E. coli* for HCT116 cell infection

The *clb*$^+$ *E. coli* BW25113 was inoculated in the modified M9-CA medium and grown at 37°C for 8 hours to reach stationary phase, and then 10 ml of the *E. coli* culture was pelleted by centrifugation. The spent supernatant was removed via aspiration, and the *E. coli* pellet was resuspended into 12 ml of DMEM/F12 medium supplemented with 15 mM HEPES, 10% FBS, and 12.5 μg/ml chloramphenicol. The resuspended cells were pre-warmed at 37°C prior to use.

HCT116 cell infection experiment

The HCT116 cells were grown in T75 flasks to >80% confluence. The cultivation medium was aspirated, followed by a 1× PBS wash (2 × 10 mL). Then the HCT116 cells were infected with 12 ml of pre-warmed *clb*$^+$ *E. coli* BW25113 cells for 2 hours at 37°C. After the infection was completed, the HCT116 cells were washed with 1× PBS (2 × 10 mL), trypsinized, and centrifuged at 300 × g for 4 min at room temperature. The supernatant was removed via aspiration, and the remaining HCT116 cell pellet was washed twice with 1.5 mL of 1× PBS with cell recovery at 250 × g for 4 min at room temperature. The cell pellets were then resuspended in 1× PBS for genomic DNA isolation.

Genomic DNA isolation and reprecipitation

The genomic DNA was isolated using the DNeasy Blood and Tissue Kit (Qiagen, Hilden, Germany) following the manufacturer's instructions. After the DNA was eluted, DNA was reprecipitated to remove the remaining detergent residue from the kit. To reprecipitate the genomic DNA, 90 μL of 1 M sodium chloride was added into 360 μL of eluted genomic DNA, followed by addition of 1050 μL of 100% ethanol. The mixture was briefly vortexed and then incubated at −20°C for 2 hours. The resulting DNA precipitant was pelleted via centrifugation (14,000 × g, 5 min, 4°C). The DNA pellet was further washed using 70% ethanol (1.5 mL × 2) and pelleted via centrifugation (14,000 × g, 5 min, 4°C). The supernatant was removed via aspiration. The post-washed DNA pellet was air dried at room temperature for 30 min and resuspended in water prior to digestion.

DNA digestion

DNA was digested using the Nucleoside Digestion Mix (New England Biolabs) in 1 hour at 37°C. Alternatively, DNA was digested in the stepwise method using NEBuffer 1.1 (10 mM Bis-Tris-Propane-HCl, 10 mM magnesium chlorids, 100 μg/ml BSA, pH 7 New England Biolabs) supplemented with 0.5 mM calcium chloride and 0.5 mM zinc chloride. First 2 units/μg DNA of DNase I (New England Biolabs) was added to the genomic DNA, and the digestion occurred at 37°C for 1 hour. Then 10 units/μg of Nuclease P1 (New England Biolabs) was added to the digestion mix, and the second step digestion lasted at 37°C for 1 hour. Finally, 1 unit/μg DNA of Quick Dephosphorylation Kit (New England Biolabs) was added to the digestion mix, and the third step digestion lasted at 37°C for 30 min.

Sample preparation for colibactin (17) and S34

Single colonies of *E. coli* DH10B *clb*$^-$, *E. coli* DH10B *clb*$^+$, *E. coli* DH10B Δ*clbO*, and *E. coli* DH10B Δ*clbL*-S179A were individually used to inoculate of 5 mL of LB with chloramphenicol (12.5 μg/mL). After incubation at 37°C with 250 rpm for 20 hours, 25 μL of each seed culture was used to inoculate 5 mL of 3 replicates of 5 mL of production media described above. The cultures were grown at 37°C with 250 rpm to an OD_{600} of 0.4 to 0.6 and cooled on ice for 10 min before inducing with isopropyl β-D-1-galactopyranoside (IPTG) at a final concentration of 0.2 mM. After cultures were incubated at 25°C with 250 rpm for 42 hours 6 mL of ethyl acetate was added to each culture. The cultures were vortexed for 20 s and separated by centrifugation (1500 × g for 10 min). The 5 mL of ethyl acetate was transferred and removed in vacuo. The dried extracts were dissolved in 100 μL of methanol for LC-HRMS analysis. Similar sample preparation method was performed from *E. coli* Nissle 1917, *E. coli* Nissle 1917 Δ*clb*, and *E. coli* Nissle 1917 Δ*clbS* strains with some modification. Overnight cultures were prepared with a different antibiotic, spectinomycin (100 μg/mL), for *E. coli* Nissle 1917 Δ*clbS*, or without antibiotic for *E. coli* Nissle 1917 and *E. coli* Nissle 1917 Δ*clb*. 25 μL of each seed culture was used to inoculate 5 mL of 3 replicates of 5 mL of production media. The cultures were grown at 37°C with 250 rpm for 48 hours before LC-HRMS samples were prepared as described above. Samples for isotopic labeling analysis were prepared from *E. coli* Nissle 1917 Δ*clbS* with L-[U-^{13}C]-Ala, Met, Gly, or Cys, and *E. coli* DH10B *clb*$^+$ with [U-^{13}C]-Gly.

Sample preparation for precolibactin 1489 (18)

The same method of colibactin (**17**) and **S34** was used for sample preparation of precolibactin 1489 (**18**) with a different strain, *E. coli* DH10B Δ*clbP*-S95A.

Dose-dependent cross-linking assay using the synthetic intermediate 38

A sample of **38** was diluted in DMSO such that each reaction consisted of a fixed 5% DMSO final concentration. 200 ng (15.4 μM in base pairs) of linearized pUC19 DNA as prepared above was added into every reaction with a total volume of 20 μL. The final concentration of **38** was adjusted to 200 μM, 100 μM, 10 μM, 1 μM, and 100 nM (absolute concentrations of **38** were approximate). 100 μM cisplatin was used as the positive control, and 5% DMSO was used as the negative control. Pure cisplatin (Biovision) stock solutions were diluted into DMSO immediately before use. All reactions were carried out in 10 mM sodium citrate pH 5.0 buffer and incubated for 3 hours at 37°C. The DNA was immediately analyzed by gel electrophoresis after incubation.

pH-dependent cross-linking assay using the synthetic intermediate 38

A sample of **38** was diluted in DMSO such that each reaction consisted of a fixed 5% DMSO final concentration. 200 ng (15.4 μM in base pairs) of linearized pUC19 DNA was added into every reaction with a total volume of 20 μL. The final concentration of **38** was adjusted to 100 μM (absolute concentrations of **38** were approximate). Reactions were conducted using the following buffer conditions with pH ranging from 5.0 to 7.4: 10 mM sodium citrate (pH 5.0), 10 mM sodium acetate (pH 5.5), 10 mM sodium citrate (pH 6.0), 10 mM sodium citrate (pH 6.5), 10 mM sodium phosphate (pH 7.0), and 10 mM sodium phosphate (pH 7.4). 100 μM cisplatin was used as the positive control, and 5% DMSO was used as the negative control. Both of these control reactions were carried out in 10 mM Tris–1 mM EDTA (pH 8.0) buffer. Pure cisplatin (Biovision) stock solutions were diluted into DMSO immediately prior to use. All of the reactions were incubated for 3 hours at 37°C. The DNA was immediately analyzed by gel electrophoresis after incubation.

Preparation of cross-linked DNA using the synthetic intermediate 38

A sample of **38** was diluted in DMSO and water such that the reaction consisted of a final concentration of 0.28% DMSO. 2400 ng (15.4 μM in base pairs) of linearized pUC19 DNA was added into every reaction with a total volume of 240 μL. The final concentration of **38** was adjusted to 25 μM (absolute concentrations of **38** were approximate). The reaction was conducted in 10 mM sodium citrate (pH 5.0) buffer, and incubated for 4 hours at 37°C. The DNA was repurified from the reaction mix using the Monarch PCR and DNA Cleanup Kit (New England Biolabs) and eluted using ultra purified water (Invitrogen). The isolated DNA was stored at −20°C, until further use. To prepare the positive control for cross-linked DNA, 200 ng of linearized pUC19 DNA was treated with 100 μM of cisplatin (Biovision) in 10 mM sodium citrate (pH 5.0) buffer

with 0.28% final DMSO concentration. Cross-linking with cisplatin was conducted for 4 hours at 37°C. To verify the presence of a DNA cross-link, a small quantity of DNA was analyzed by denaturing electrophoresis.

DNA gel electrophoresis for cross-linking assays

For each DNA sample, the concentration was pre-adjusted to 10 ng/μL. For non-denatured native gels, 4 μL (40 ng) of DNA was taken out and mixed with 1.5 μL of 6× purple gel loading dye, no SDS (NEB). The mixed DNA samples were immediately loaded onto 1% agarose TBE gels, and the gel was run for 1.5 hours at 90 V. The gel was post stained with SybrGold (Thermo Fisher) for 2 hours. For denaturing gels, 5 μL (50 ng) of DNA was taken out each time and separately mixed with 15 μL of 0.2% denaturing buffer (0.27% sodium hydroxide, 10% glycerol, 0.013% bromophenol blue), 0.4% denaturing buffer (0.53% sodium hydroxide, 10% glycerol, 0.013% bromophenol blue), or 1% denaturing buffer (1.33% sodium hydroxide, 10% glycerol, 0.013% bromophenol blue) at 0°C. The mixed DNA samples were denatured at 4°C for 10 min and immediately loaded onto 1% agarose TBE gels. The gel was run for 1.5 hours at 90 V. The gel was post stained with SybrGold (Thermo Fisher) for 2 hours.

Digestion of DNA cross-linked by 38

Following gel verification of the DNA cross-link, 2000 ng of the remaining DNA was digested using the Nucleoside Digestion Mix (New England Biolabs) for 1 hour at 37°C. The digested DNA was stored at −80°C prior to MS analysis.

General synthetic procedures

All reactions were performed in single-neck, flame-dried, round-bottomed flasks fitted with rubber septa under a positive pressure of nitrogen unless otherwise noted. Air- and moisture-sensitive liquids were transferred via syringe or stainless steel cannula, or were handled in a nitrogen-filled drybox (working oxygen level <10 ppm). Organic solutions were concentrated by rotary evaporation at 28 to 32°C. Flash-column chromatography was performed as described by Still *et al*. (*45*), employing silica gel (60 Å, 40 to 63 μm particle size) purchased from Sorbent Technologies (Atlanta, GA). Analytical thin-layered chromatography (TLC) was performed using glass plates pre-coated with silica gel (0.25 mm, 60 Å pore size) impregnated with a fluorescent indicator (254 nm). TLC plates were visualized by exposure to ultraviolet light (UV).

Materials

Commercial solvents and reagents were used as received with the following exceptions. Dichloromethane, ether, and *N*,*N*-dimethylformamide were purified according to the method of Pangborn *et al*. (*46*) Triethylamine was distilled from calcium hydride under an atmosphere of argon immediately before use. Di-*iso*-propylamine was distilled from calcium hydride and was stored under nitrogen. Methanol was distilled from magnesium turnings under an atmosphere of nitrogen immediately before use. Tetrahydrofuran was distilled from sodium–benzophenone under an atmosphere of nitrogen immediately before use. Commercial solutions of lithium di-*iso*-propyl amide in tetrahydrofuran–heptane–ethylbenzene were titrated by a variation of the procedure of Ireland and Meissner (*47*) using menthol and 1,10-phenanthroline. The β-ketothioester **27** was prepared according to a published procedure (*17*).

REFERENCES AND NOTES

1. N. K. Surana, D. L. Kasper, Moving beyond microbiome-wide associations to causal microbe identification. *Nature* **552**, 244–247 (2017). doi: 10.1038/nature25019; pmid: 29211710
2. M. A. Fischbach, Microbiome: Focus on causation and mechanism. *Cell* **174**, 785–790 (2018). doi: 10.1016/j.cell.2018.07.038; pmid: 30096310
3. J. R. Johnson, B. Johnston, M. A. Kuskowski, J. P. Nougayrede, E. Oswald, Molecular epidemiology and phylogenetic distribution of the *Escherichia coli* pks genomic island. *J. Clin. Microbiol.* **46**, 3906–3911 (2008). doi: 10.1128/JCM.00949-08; pmid: 18945841
4. J. Putze *et al*., Genetic structure and distribution of the colibactin genomic island among members of the family Enterobacteriaceae. *Infect. Immun.* **77**, 4696–4703 (2009). doi: 10.1128/IAI.00522-09; pmid: 19720753
5. J.-P. Nougayrède *et al*., *Escherichia coli* induces DNA double-strand breaks in eukaryotic cells. *Science* **313**, 848–851 (2006). doi: 10.1126/science.1127059; pmid: 16902142
6. G. Cuevas-Ramos *et al*., *Escherichia coli* induces DNA damage in vivo and triggers genomic instability in mammalian cells. *Proc. Natl. Acad. Sci. U.S.A.* **107**, 11537–11542 (2010). doi: 10.1073/pnas.1001261107; pmid: 20534522
7. J. C. Arthur *et al*., Intestinal inflammation targets cancer-inducing activity of the microbiota. *Science* **338**, 120–123 (2012). doi: 10.1126/science.1224820; pmid: 22903521
8. A. Cougnoux *et al*., Bacterial genotoxin colibactin promotes colon tumour growth by inducing a senescence-associated secretory phenotype. *Gut* **63**, 1932–1942 (2014). doi: 10.1136/gutjnl-2013-305257; pmid: 24658599
9. S. Tomkovich *et al*., Locoregional effects of microbiota in a preclinical model of colon carcinogenesis. *Cancer Res.* **77**, 2620–2632 (2017). doi: 10.1158/0008-5472.CAN-16-3472; pmid: 28416491
10. E. Buc *et al*., High prevalence of mucosa-associated *E. coli* producing cyclomodulin and genotoxin in colon cancer. *PLOS ONE* **8**, e56964 (2013). doi: 10.1371/journal.pone.0056964; pmid: 23457644
11. E. P. Trautman, J. M. Crawford, Linking biosynthetic gene clusters to their metabolites via pathway-targeted molecular networking. *Curr. Top. Med. Chem.* **16**, 1705–1716 (2016). pmid: 26456470
12. E. P. Balskus, Colibactin: Understanding an elusive gut bacterial genotoxin. *Nat. Prod. Rep.* **32**, 1534–1540 (2015). doi: 10.1039/C5NP00091B; pmid: 26390983
13. F. Taieb, C. Petit, J. P. Nougayrède, E. Oswald, The enterobacterial genotoxins: Cytolethal distending toxin and colibactin. *Ecosal Plus* **7**, (2016). doi: 10.1128/ecosalplus.ESP-0008-2016; pmid: 27419387
14. A. R. Healy, S. B. Herzon, Molecular basis of gut microbiome-associated colorectal cancer: A synthetic perspective. *J. Am. Chem. Soc.* **139**, 14817–14824 (2017). doi: 10.1021/jacs.7b07807; pmid: 28949546
15. T. Faïs, J. Delmas, N. Barnich, R. Bonnet, G. Dalmasso, Colibactin: More than a new bacterial toxin. *Toxins (Basel)* **10**, 151 (2018). doi: 10.3390/toxins10040151; pmid: 29642622
16. M. I. Vizcaino, J. M. Crawford, The colibactin warhead crosslinks DNA. *Nat. Chem.* **7**, 411–417 (2015). doi: 10.1038/nchem.2221; pmid: 25901819
17. A. R. Healy, H. Nikolayevskiy, J. R. Patel, J. M. Crawford, S. B. Herzon, A mechanistic model for colibactin-induced genotoxicity. *J. Am. Chem. Soc.* **138**, 15563–15570 (2016). doi: 10.1021/jacs.6b10354; pmid: 27934011
18. C. A. Brotherton, E. P. Balskus, A prodrug resistance mechanism is involved in colibactin biosynthesis and cytotoxicity. *J. Am. Chem. Soc.* **135**, 3359–3362 (2013). doi: 10.1021/ja312154m; pmid: 23406518
19. X. Bian *et al*., In vivo evidence for a prodrug activation mechanism during colibactin maturation. *ChemBioChem* **14**, 1194–1197 (2013). doi: 10.1002/cbic.201300208; pmid: 23744512
20. M. I. Vizcaino, P. Engel, E. Trautman, J. M. Crawford, Comparative metabolomics and structural characterizations illuminate colibactin pathway-dependent small molecules. *J. Am. Chem. Soc.* **136**, 9244–9247 (2014). doi: 10.1021/ja503450q; pmid: 24932672
21. X. Bian, A. Plaza, Y. Zhang, R. Müller, Two more pieces of the colibactin genotoxin puzzle from *Escherichia coli* show incorporation of an unusual 1-aminocyclopropanecarboxylic acid moiety. *Chem. Sci.* **6**, 3154–3160 (2015). doi: 10.1039/C5SC00101C; pmid: 28706687
22. C. A. Brotherton, M. Wilson, G. Byrd, E. P. Balskus, Isolation of a metabolite from the *pks* island provides insights into colibactin biosynthesis and activity. *Org. Lett.* **17**, 1545–1548 (2015). doi: 10.1021/acs.orglett.5b00432; pmid: 25753745
23. D. Dubois *et al*., ClbP is a prototype of a peptidase subgroup involved in biosynthesis of nonribosomal peptides. *J. Biol. Chem.* **286**, 35562–35570 (2011). doi: 10.1074/jbc.M111.221960; pmid: 21795676
24. A. Cougnoux *et al*., Analysis of structure-function relationships in the colibactin-maturating enzyme ClbP. *J. Mol. Biol.* **424**, 203–214 (2012). doi: 10.1016/j.jmb.2012.09.017; pmid: 23041299
25. E. P. Trautman, A. R. Healy, E. E. Shine, S. B. Herzon, J. M. Crawford, Domain-targeted metabolomics delineates the heterocycle assembly steps of colibactin biosynthesis. *J. Am. Chem. Soc.* **139**, 4195–4201 (2017). doi: 10.1021/jacs.7b00659; pmid: 28240912
26. M. Xue, E. E. Shine, W. Wang, J. M. Crawford, S. B. Herzon, Characterization of natural colibactin-nucleobase adducts by tandem mass spectrometry and isotopic labeling. Support for DNA alkylation by cyclopropane ring opening. *Biochemistry* **57**, 6391–6394 (2018). doi: 10.1021/acs.biochem.8b01023; pmid: 30365310
27. M. R. Wilson *et al*., The human gut bacterial genotoxin colibactin alkylates DNA. *Science* **363**, eaar7785 (2019). doi: 10.1126/science.aar7785; pmid: 30765538
28. N. Bossuet-Greif *et al*., The colibactin genotoxin generates DNA interstrand cross-links in infected cells. *mBio* **9**, e02393-17 (2018). doi: 10.1128/mBio.02393-17; pmid: 29559578
29. Z. R. Li *et al*., Critical intermediates reveal new biosynthetic events in the enigmatic colibactin pathway. *ChemBioChem* **16**, 1715–1719 (2015). doi: 10.1002/cbic.201500239; pmid: 26052818
30. A. R. Healy, M. I. Vizcaino, J. M. Crawford, S. B. Herzon, Convergent and modular synthesis of candidate precolibactins. Structural revision of precolibactin A. *J. Am. Chem. Soc.* **138**, 5426–5432 (2016). doi: 10.1021/jacs.6b02276; pmid: 27025153
31. Z. R. Li *et al*., Divergent biosynthesis yields a cytotoxic aminomalonate-containing precolibactin. *Nat. Chem. Biol.* **12**, 773–775 (2016). doi: 10.1038/nchembio.2157; pmid: 27547923
32. L. Zha, M. R. Wilson, C. A. Brotherton, E. P. Balskus, Characterization of polyketide synthase machinery from the *pks* island facilitates isolation of a candidate precolibactin. *ACS Chem. Biol.* **11**, 1287–1295 (2016). doi: 10.1021/acschembio.6b00014; pmid: 26890481
33. A. R. Healy *et al*., Synthesis and reactivity of precolibactin 886. chemRxiv (2019); https://chemrxiv.org/articles/Synthesis_and_Reactivity_of_Precolibactin_886/7849151.
34. Z.-R. Li *et al*., Macrocyclic colibactin induces DNA double-strand breaks via copper-mediated oxidative cleavage. bioRxiv 530204 (2019).
35. T. Baba *et al*., Construction of *Escherichia coli* K-12 in-frame, single-gene knockout mutants: The Keio collection. *Mol. Syst. Biol.* **2**, 0008 (2006). doi: 10.1038/msb4100050; pmid: 16738554
36. L. Zha *et al*., Colibactin assembly line enzymes use *S*-adenosylmethionine to build a cyclopropane ring. *Nat. Chem. Biol.* **13**, 1063–1065 (2017). doi: 10.1038/nchembio.2448; pmid: 28805802
37. A. O. Brachmann *et al*., Colibactin biosynthesis and biological activity depend on the rare aminomalonyl polyketide precursor. *Chem. Commun.* **51**, 13138–13141 (2015). doi: 10.1039/C5CC02718G; pmid: 26191546
38. N. S. Guntaka, A. R. Healy, J. M. Crawford, S. B. Herzon, S. D. Bruner, Structure and functional analysis of ClbQ, an unusual intermediate-releasing thioesterase from the colibactin biosynthetic pathway. *ACS Chem. Biol.* **12**, 2598–2608 (2017). doi: 10.1021/acschembio.7b00479; pmid: 28846367

39. Y. Jiang *et al*., The reactivity of an unusual amidase may explain colibactin's DNA cross-linking activity. bioRxiv 567248 [Preprint] 4 March 2019. https://doi.org/10.1101/567248.
40. Y. Jiang *et al*., Reactivity of an unusual amidase may explain colibactin's DNA cross-linking activity. *J. Am. Chem. Soc.* **141**, 11489–11496 (2019). doi: 10.1021/jacs.9b02453; pmid: 31251062
41. E. E. Shine *et al*., Model colibactins exhibit human cell genotoxicity in the absence of host bacteria. *ACS Chem. Biol.* **13**, 3286–3293 (2018). doi: 10.1021/acschembio.8b00714; pmid: 30403848
42. P. Tripathi *et al*., ClbS is a cyclopropane hydrolase that confers colibactin resistance. *J. Am. Chem. Soc.* **139**, 17719–17722 (2017). doi: 10.1021/jacs.7b09971; pmid: 29112397
43. R. P. Bell, in *Advances in Physical Organic Chemistry*, V. Gold, Ed. (Academic Press, 1966), vol. 4, pp. 1–29.
44. N. Bossuet-Greif *et al*., *Escherichia coli* ClbS is a colibactin resistance protein. *Mol. Microbiol.* **99**, 897–908 (2016). doi: 10.1111/mmi.13272; pmid: 26560421
45. W. C. Still, M. Kahn, A. Mitra, Rapid chromatographic technique for preparative separations with moderate resolutions. *J. Org. Chem.* **43**, 2923–2925 (1978). doi: 10.1021/jo00408a041
46. A. B. Pangborn, M. A. Giardello, R. H. Grubbs, R. K. Rosen, F. J. Timmers, Safe and convenient procedure for solvent purification. *Organometallics* **15**, 1518–1520 (1996). doi: 10.1021/om9503712
47. R. E. Ireland, R. S. Meissner, Convenient method for the titration of amide base solutions. *J. Org. Chem.* **56**, 4566–4568 (1991). doi: 10.1021/jo00014a050

ACKNOWLEDGMENTS

Funding: Financial support from the National Institutes of Health (R01GM110506 to S.B.H., 1DP2-CA186575 to J.M.C., and R01CA215553 to S.B.H. and J.M.C.), the Chemistry Biology Interface Training Program (T32GM067543 to K.M.W.), the Charles H. Revson foundation (postdoctoral fellowship to A.R.H.), the NSF graduate research fellowship program (E.E.S), and Yale University is gratefully acknowledged. The structure of colibactin (**17**) was first disclosed by S.B.H. on 3 December 2018 at the Merck Lecture, Department of Chemistry, The University of Illinois, Urbana-Champaign; by J.M.C. on 11 February 2019 at a Departmental Symposium, Department of Chemistry, Massachusetts Institute of Technology; and by M.X. on 11 March 2019 during a lecture entitled "Characterization of natural colibactin nucleobase adducts by tandem MS and isotopic labeling" at the Keystone Symposia meeting "Microbiome: Chemical mechanisms and biological consequences." **Author contributions:** M.X. discovered and characterized the natural colibactin-diadenine adduct **9**, conducted tandem MS analysis of synthetic colibactin-DNA adducts, carried out bacterial infection studies, and identified the colibactin-adenine adducts **9**, **S1**, **4**, and **14** in genomic DNA; C.S.K. characterized natural colibactin (**17**) and precolibactin 1489 (**18**) in bacterial extracts; A.R.H. contributed to the conception of the synthesis, conducted preliminary synthetic studies, and suggested protection of the fragment coupling product **24** as its enoxysilane; K.M.W. conceived the twofold coupling approach to colibactin, developed a synthesis of the β-ketothioeseter **25**, and optimized the synthetic route; Z.W. optimized the synthetic route and completed the synthesis of colibactin; M.C.F. developed a scalable synthetic route to the α-nitroketone **33**; E.E.S. generated new strains, contributed to the bacterial infection studies, and developed the *clbS* mutant strategy to enhance detection of natural colibactin; and W.W. assisted with tandem MS analysis of DNA-colibactin adducts. S.B.H. and J.M.C. conceived the study, oversaw experiments, and wrote the manuscript. **Competing interests:** The authors declare no competing interests. **Data availability:** All data to support the conclusions of this manuscript are included in the main text or supplementary materials.

SUPPLEMENTARY MATERIALS

science.sciencemag.org/content/365/6457/eaax2685/suppl/DC1
Supplementary Text
Figs. S1 to S156
Tables S1 to S78
NMR Spectra

7 March 2019; accepted 24 July 2019
Published online 8 August 2019
10.1126/science.aax2685

Science

Structure elucidation of colibactin and its DNA cross-links

Mengzhao Xue, Chung Sub Kim, Alan R. Healy, Kevin M. Wernke, Zhixun Wang, Madeline C. Frischling, Emilee E. Shine, Weiwei Wang, Seth B. Herzon and Jason M. Crawford

Science **365** (6457), eaax2685.
DOI: 10.1126/science.aax2685originally published online August 8, 2019

Double warhead does DNA damage

Strains of the human gut bacterium *Escherichia coli* carrying the *clb* gene cluster produce a secondary metabolite dubbed colibactin and have been provocatively linked to colorectal cancer in some models. Colibactin has been difficult to isolate in full, but pieces of the structure have been worked out, including an electrophilic warhead. Xue *et al.* found that colibactin contains two conjoined warheads, which is consistent with its ability to alkylate and cross-link DNA. Chemical synthesis and comparison to cell coculture confirm the structure and properties of this unstable and potentially carcinogenic metabolite.

Science, this issue p. eaax2685